AD-A141 272 THE INFLUENCE OF LATTICE IMPERFECTIONS ON THE CHEMICAL REACTIVITY OF SOLI..(U) UNIVERSITY OF STRATHCLYDE GLASGOW (SCOTLAND) DEPT OF PURE AND.. 1/1

UNCLASSIFIED J N SHERWOOD ET AL. FEB 84 DAERO-78-G-078 F/G 20/2 NL

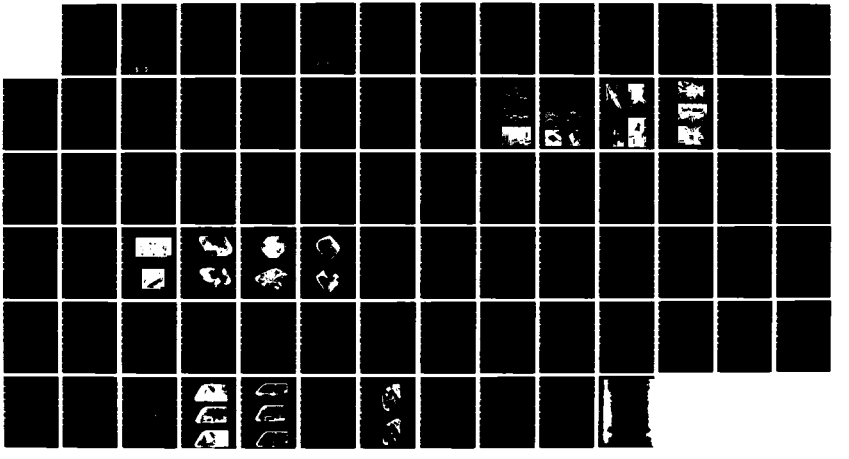

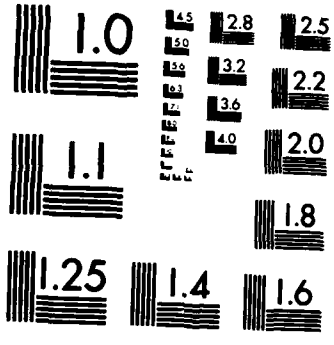

MICROCOPY RESOLUTION TEST CHART
NATIONAL BUREAU OF STANDARDS-1963-A

AD-A141 272

R&D 2376-CH (11)

AD

THE INFLUENCE OF LATTICE IMPERFECTIONS ON THE CHEMICAL REACTIVITY OF SOLIDS

THE GROWTH, PERFECTION AND DEFECT PROPERTIES OF PETN AND RDX SINGLE CRYSTALS

by

John N. Sherwood
Peter J. Halfpenny
Kevin J. Roberts

FINAL REPORT (PART II)

FEBRUARY 1984

United States Army

EUROPEAN RESEARCH OFFICE FOR THE U.S. ARMY

London England

CONTRACT NUMBER DAERO-78-G-078

Professor John N. Sherwood
University of Strathclyde

Approved for Public Release; distribution unlimited

DTIC FILE COPY

DTIC ELECTE MAY 18 1984 S D

B

84 05 14 030

UNCLASSIFIED
SECURITY CLASSIFICATION OF THIS PAGE (When Data Entered)

REPORT DOCUMENTATION PAGE		READ INSTRUCTIONS BEFORE COMPLETING FORM
1. REPORT NUMBER	2. GOVT ACCESSION NO. AD-A141272	3. RECIPIENT'S CATALOG NUMBER
4. TITLE (and Subtitle) The Influence of Lattice Imperfections on the Chemical Reactivity of Solids.		5. TYPE OF REPORT & PERIOD COVERED FINAL TECHNICAL
		6. PERFORMING ORG. REPORT NUMBER
7. AUTHOR(s) J. N. Sherwood		8. CONTRACT OR GRANT NUMBER(s) DAERO-78-G-078
9. PERFORMING ORGANIZATION NAME AND ADDRESS University of Strathclyde Department of Pure and Applied Chemistry Glasgow, G1 1XL, SCOTLAND		10. PROGRAM ELEMENT, PROJECT, TASK AREA & WORK UNIT NUMBERS 6.11.02A 1T16 1102BH57-02
11. CONTROLLING OFFICE NAME AND ADDRESS USARDSG (UK) Box 65 FPO, New York 09510		12. REPORT DATE FEBRUARY 1984
		13. NUMBER OF PAGES 137
14. MONITORING AGENCY NAME & ADDRESS (if different from Controlling Office) U. S. Army Research Office P. O. Box 12211 Research Triangle Park, NC		15. SECURITY CLASS. (of this report) UNCLASSIFIED
		15a. DECLASSIFICATION/DOWNGRADING SCHEDULE

16. DISTRIBUTION STATEMENT (of this Report)
Approved for Public Release; Distribution Limited
UN

17. DISTRIBUTION STATEMENT (of the abstract entered in Block 20, if different from Report)

18. SUPPLEMENTARY NOTES

19. KEY WORDS (Continue on reverse side if necessary and identify by block number)
Energetic materials, Detonation, PETN, RDX, HMX, Single crystals, Crystal growth, Crystal perfection, Dislocations, Mechanical properties, Dislocation slip, Twinning, Polymorphism, Mechanical deformation.

20. ABSTRACT (Continue on reverse side if necessary and identify by block number)
This report presents an assessment of the growth and perfection of single crystals of the secondary explosive materials PETN and RDX. An account is also given of some preliminary studies of their mechanical behaviour.

Details are presented for the preparation of large single crystals of PETN and RDX of extremely high perfection. Using the techniques of X-ray diffraction topography coupled where possible with theoretical calculations, an analysis is made of the dominant growth defect structure of these materials.
cont ...

DD FORM 1 JAN 73 1473 EDITION OF 1 NOV 65 IS OBSOLETE

In both cases the principal defects are dislocations. There is also evidence of growth twinning in PETN. The character (line direction and Burgers vector) of the dislocations are defined. Burgers vectors up to and including lattice translations of <111> (PETN) and <110> (RDX) were identified.

Initial attempts have been made to examine the mechanical properties of PETN and RDX using microhardness indentation, etching techniques and X-ray topography. The results are used to make an appraisal of the likely dominant mechanical deformation processes. These are

PETN - microtwinning and dislocation slip on {110} slip planes, Burgers vector b [001].

RDX - dislocation slip on (010) (dominant) and possibly also on (011) or (021) and (001) slip planes, Burgers vectors on (010); b[100] and on (001); b[010] and b[110].

PART II

CONTENTS

REPORT

Studies of the Growth, Perfection and Defect Properties of Pentaerythritol Tetranitrate (PETN) and Cyclotrimethylene Trinitramine (RDX)

Comprising a series of five papers to be published under the series title DISLOCATIONS IN ENERGETIC MATERIALS. Each paper is separately numbered.

Part I contains the Introduction and first two papers.

Part II contains the remaining papers.

DTIC
ELECTE
MAY 1 8 1984
S D
B

Accession For
NTIS GRA&I
DTIC TAB
Unannounced
Justification
PER FORM 50
By
Distribution/
Availability Codes
Dist | Avail and/or Special
A-1

DTIC COPY INSPECTED

DISLOCATIONS IN ENERGETIC MATERIALS

3. Etching and Microhardness Studies of Pentaerythritol Tetranitrate and Cyclotrimethylenetrinitramine.

P.J. Halfpenny[1], K.J. Roberts[2] and J.N. Sherwood

Department of Pure and Applied Chemistry
University of Strathclyde, Glasgow G1 1XL
Scotland

[1] Department of Engineering, University of Southampton, SOUTHAMPTON, SO9 5NH

[2] Institut fur Kristallographie, RWTH, Templergraben 55, D-5100 AACHEN, West Germany

ABSTRACT

An assessment has been made of the primary dislocation slip systems in the explosives pentaerythritol tetranitrate (PETN) and cyclotrimethylene trinitramine (RDX) using a combination of dislocation etching and microhardness indentation techniques.

Hardness measurements were made on all major habit faces as a function of temperature and load. These showed that, within the attainable temperature range (PETN 293-353K, RDX 293-373K) no change in hardness occurred which could be associated with the development of deformation mechanisms additional to those operating at room temperature. The hardness values of both materials were consistent with values obtained in some previous measurements (PETN 17kgmm^{-2}, RDX 39kgmm^{-2}).

Solvent etching with acetone (5s at 274K) proved to be an excellent method for revealing the emergent ends of growth and mechanically induced dislocations in PETN. Etching of microhardness indentations confirmed that observable slip traces comprised dislocations. These migrated up to 160μm (20g load) from the indentation point on both {110} and {101} faces. The alignments defined a {110} primary slip plane.

Parallel experiments with RDX yielded evidence of highly localised slip around the indentation mark (90μm, 50g load). Two alignments of etch-pits were noticeable. The better defined of these lay at the intersection of the (010) plane with the habit faces. The second could not be defined absolutely but most probably corresponds to the intersection of either the (011) or (012) plane with the surfaces.

Consideration of the Burgers vectors of dislocations which are likely to glide in these planes lead us to speculate that the primary slip systems are, PETN {110} [001] and RDX,(010) [001]. Such an assignment would be consistent with the relative hardness of the two materials.

1. INTRODUCTION

Experimental studies of the sensitivity of energetic materials to initiation by mechanical shock [1-4] has given rise to the speculation that the energy localised during the accompanying plastic deformation may contribute significantly to the initiation process. A mechanism has been proposed whereby dislocations, driven along their slip-planes by the initiating shock wave "pile-up", either against each other or some obstacle [5]. The consequent transfer of strain and kinetic energy to heat within a microscopic region is proposed to form the "hot spot" which nucleates the reaction. Theoretical calculations have been made to confirm that such a model is rational [6]. Unfortunately, little is known of the properties and characteristics of mechanically induced dislocations in this type of material and on which detailed assessments can be based. In an effort to fill this gap, we have commenced a detailed analysis of the defect properties of organic energetic materials. In the present case we detail methods for the etching of the emergent ends of dislocations in pentaerythritol tetranitrate (PETN). Using these coupled with microhardness indentation studies we define for the first time the primary slip planes in this material.

Using previously defined etching techniques a similar comparison is made for the related solid cyclotrimethylene trinitramine (RDX).

2. EXPERIMENTAL

2.1 Crystal Preparation

Crystals of PETN and RDX were grown by slow cooling of the saturated solutions of the multiply recrystallized solid from purified acetone (PETN and RDX) and ethyl acetate (PETN).[7] The crystals of both solids were prismatic and exhibited well-developed facetting. The principal forms were

PETN {110} and {101}

RDX {210}, {111}, {001}, {010}, {100} and {102}

Complete details of the purification, purity and preparation of the crystals and the variation of morphology and internal perfection with preparation conditions will be given elsewhere.[8]

The crystal structures of the two materials are as follows

PETN Tetragonal, space group $P\bar{4}2_1c$

$a = b = 0.938nm$, $c = 0.670nm$, $z = 2$ [9]

RDX Orthorhombic, space group Pbca

$a = 1.318nm$, $b = 1.157nm$, $c = 1.071$, $z = 8$ [10]

2.2 Etching Studies

2.2.1 RDX

The etchant devised by Connick and May [11], acetone at 298K, was used for this material. Etching of "as grown" surfaces produced results similar to those noted by these workers. For the etching of indentation marks it was found necessary to reduce the etching time to 1s in order to resolve individual pits.

2.2.2 PETN

As far as we are aware, only a brief note of the uncontrolled solvent etching of this material has been previously published.[12] A number of solvents and mixtures of solvents were assessed. The results are summarized in Table 1. Acetone proved to be the most satisfactory etchant. Etching was rapid however and to produce well-defined pits it was found necessary to etch for periods of <5s at 274K followed by a rapid quench in water at this temperature. The results of this procedure for both {100} and {101} habit faces are shown in Figures 1a, b and c.

Since PETN does not cleave, no comparison of etch patterns on cleavage pairs could be made. The correspondence of etch pits with dislocations is well-defined however by their persistence on repeated etching and their association with slip patterns following microhardness indentation (Figure 3).

2.3 Microhardness Measurements

Microhardness studies were carried out using a Leitz Miniload microhardness tester fitted with a Vickers pyramidal indenter. Measurements were made as a function of load, temperature and crystal orientation.

3. RESULTS

3.1 Etching Studies

3.1.1 PETN

a) {110} Faces

Figures 1a and 1b show {110} habit faces etched as described above. All pits were hexagonal in surface section and showed three geometries

Type 1 - Semi-regular hexagonal pits symmetrical about [110].

Type 2 - Hexagonal pits with {110} as the plane of symmetry but elongated in the [001] direction.

Type 3 - Irregularly shaped hexagonal pits with an axis of symmetry normal to the surface.

Flat bottomed pits were also noted.

Types 1 and 2 pits predominantly formed [001] alignments with some isolated pits. Type 3 pits were predominantly isolated.

All pits initially retained their shape on continued etching. Types 1 and 2 eventually became flat bottomed, type 3 always maintained a point bottom.

Optical and interference microscopy allowed the definition of the geometry of the type 1 and 2 pits as shown in Figure 2.

Type 1 pits are shallow with planar surfaces lying along high index planes. The point is displaced a considerable distance from the geometrical centre, indicating that the dislocation line is inclined at a low angle to the surface.

Type 2 pits are similarly shallow but have convex sides. The gradient of these increases towards the point. Although the apex is close

to the geometrical centre, the shallowness of the pit implies that the dislocation must again lie at a relative low angle to the surface. For both pits the combination of shape and alignment confirms that the dislocations must lie in the {110} planes.

Type 3 pits differ from 1 and 2 in that the point coincides with the geometrical centre. Thus the dislocation responsible emerges normal to the surface.

A survey of a large selection of etched crystals showed the incidence of pits to be Type 1 > Type 2 >> Type 3. The last form only a few percent of the total.

b) {101} Faces

Etch-pits on these faces were all similarly trapezoidal in surface shape and formed alignments parallel to the intersection of the {110} planes with the face (Figure 1c). In all cases the points were offset from the geometrical centre (Figure 2c). The offset angle varied from pit to pit and it was not possible to obtain sufficient definition for interference microscopy. General observation indicated that the dislocation lines must lie in the {110} planes.

c) Possible Dislocation Types

Three types of growth dislocations in the {110} growth sector have been identified by X-ray topography [13]; $\underline{b}$[001] edge, $\underline{b}$<100> mixed and $\underline{b}$<111> mixed. Of these, only those with $\underline{b}$[001] lie normal to the surface and could yield a pit of Type 3 geometry. The persistence of this type of pit on continued etching, the small numbers and the fact that it does not usually form part of any alignment is consistent with this interpretation. The other growth dislocations are more highly inclined; $\underline{b}$<100> in the (001) plane at 68° to (110) and b<111> in the {110} plane at 70° to the face. Pits associable with the former geometry have not been noted. The latter could yield a pit of Type 1 or 2 geometry and some of the isolated pits could represent these dislocations. For the most part however it is

probable that the majority of the Types 1 and 2 pits result from dislocations mechanically induced by surface damage during growth and preparation, and which lie in {110} slip planes. Their total numbers far exceed the bulk dislocation content as evidenced by X-ray topography ($<10cm^{-3}$). Their alignment and the fact that on continued etching, they develop a flat bottom also is consistent with this interpretation. If so, the low angle to the surface implies only a shallow penetration of the dislocation loops.

Whether or not the types 1 and 2 pits reflect different dislocation types, differences in etching rates or simply different depths of the dislocation loops is difficult to assess. Their distinctive orientation coupled with their close proximity on the surface does suggest that they result from different mechanical dislocation types.

Confirmation of the mechanical genesis of the majority of etch pits can be derived from the etching studies of the {101} faces. From the topographic studies [12] we know these growth sectors to be highly perfect and the lack of etch pits associable with growth dislocations is not surprising. All etch pits form arrays consistent with shallow, mechanically induced, dislocation loops lying close to the surface in the {110} planes.

In summary, etch patterns on PETN crystal surfaces and their geometries are consistent with the emergence points of known growth dislocation types and with mechanically induced dislocations which glide on {110} slip planes. Further evidence for the latter can be adduced from microhardness measurements.

3.2 Deformation Studies

3.2.1 Microhardness Measurements

Previous studies of the microhardness of these materials were directed towards the definition of surface energy and crack formation.[14] In these studies evidence for slip in PETN was noted. We have extended

this type of measurement in an effort to define the dislocations involved in the process.

a) PETN

The hardness of 'as grown' {110} and {101} type crystal surfaces was determined as a function of load ({110} and {101}) and temperature, {110}. Indentations made as a function of orientation in the surface revealed slip traces characteristic of localised plastic deformation around the indentation mark together with some cracking (Figure 3a and c). Both slip and crack directions were constant, independent of orientation. The cracks duplicated, in size and orientation, the observations of Hagan and Chaudhri [14] and were not studied further.

Even with careful surface orientation the indentations were not square and straight-sided. This is indirect evidence of anisotropy. The slip patterns produce a curved trough on the surface which distorts the indentation and leads to errors in the measurement. Further errors may also arise as a consequence of the propagation of the surface cracks which will use energy which might otherwise have been utilised in plastic flow. To minimise these errors and to produce comparative data, hardness measurements on {110} surfaces were made with one indenter diagonal parallel to [001] and using the length of the <110> diagonal in the calculations. For similar reasons all measurements on the {101} faces were taken with one diagonal parallel to the trace of [110] on this face.

There was no variation in hardness with load or surface orientation within experimental error. The range, Diamond Pyramidal Hardness, DPH = 15-17kgmm^{-2} was in satisfactory agreement with a value quoted by Hagan and Chaudrhi.

The lack of variation with load is not surprising. If two indentations have the same shape, then whatever their size, the associated strain field will be identical. Thus hardness will be independent of load. In contrast, variation of hardness with surface orientation is

usually expected by virtue of the orientation of the indenter with respect to the slip systems presented on each face. We can only assume that the difference in angle between the direction of indentation and slip plane is compensated for by that between the indentation direction and slip direction or by the availability of two slip systems on the {101} faces.

The variation in hardness with temperature was small but significant; DPH = 17-13kgmm^{-2} over the range 298-323K. The decrease was gradual and is probably consistent with changes in intermolecular lattice forces with temperature. From this and surface observations, we conclude that only the slip systems operative at ambient temperature remain so up to 323K. At this temperature surface deterioration due to evaporation and decomposition commences.

b) RDX

Hardness measurements were made as a function of load and temperature on the {210} faces of RDX. As noted by Hagan and Chaudhri [14] extensive cracking parallel and perpendicular to [001] accompanied all indentations.

No slip lines were observable over the range of loads used. The hardness remained constant with load (DPH = 38-39kgmm^{-2}) but exhibited a smooth decrease with temperature (39-27kgmm^{-2}) in the range 294-373K. Thus it is unlikely that there will be any sudden changes in deformation mechanisms over this range. The hardness value of 39kgmm^{-2} (294K) is much higher than that noted by Hagan and Chaudhri (24kgmm^{-2}) and corresponds to the upper end of a range noted by Elban and Armstrong [15] (32-39kgmm^{-2}). We attribute this to the improved quality of crystals used in the present study.

3.2.2 Etching of Microhardness Indentations

The indented faces of both PETN and RDX crystals were etched in order to define more clearly the full extent of the plastically deformed regions around the indentations and to provide more information on the densities and configurations of dislocations in these slip planes.

a) PETN

Figures 3b and 3d show etched indentations (20g load) on the (110) and (101) faces respectively. In the former case, type 1 dislocation etch-pits spread out from the indentation in lines corresponding to the intersection of a $(1\bar{1}0)$ plane with the surface. Interestingly, the pit-bottoms show a similar oblique orientation to the surface on both sides of the indentation mark suggesting, that they represent the ends of oblique loops of a parallelogram shape. This alignment and the pit orientation define a (110) slip plane.

This geometry is confirmed by the distribution of pits around the indentation on the (101) face (Figure 3d). These lie in alignments corresponding to the intersection of the (110) and $(1\bar{1}0)$ planes with the face. Again the pits show equivalent assymetry on both sides of the loop. They also show an interesting distribution on each side of the indentation giving a short and long arm in each 'quadrant' implying a considerable anisotropy of the slip process.

b) RDX

Etched indentations (50g load) on the {210}, {111} and (001) habit faces are depicted in Figures 4a, b and c. Despite the fact that no slip lines were apparent during the microhardness studies, all reveal dislocation alignments spreading for small distances around the marks.

On the {210} face the dominant alignment is in the [001] direction. It is interesting to note that the rows of pits propagate from the crack C rather than from the indentation itself. Also, they are on one side of the indentation only. This reflects the crystallographic symmetry of the (210) face. A second possible alignment at 30- 60° to [001] can also be detected at A.

The result of etching an indentation on the (001) face (Figure 4b) is to yield alignments parallel to [100]. Only one plane, namely (010), could give rise to the principal alignments on the (210) and (001) faces. This

defines the slip plane. This assignment is confirmed by the etched indentation on the (111) face where again alignments are produced which correspond to the trace of the (010) plane on this surface.

Although there is some confusion in the latter case due to the etching of cracks which inevitably accompanied indentation on this face, there is a definite indication of a secondary alignment at X. Accepting that this is present and returning to Figure 4a we note that the most probable orientation of alignment A is parallel to the intersection of either the (021) or (011) plane with the face. Both of these planes will intersect the (001) faces in a line parallel to [100] and hence yield no additional alignment. Their intersection with the (111) face are noted on Figure 4c. Of the two possibilities, this evidence suggests that the most likely secondary slip plane is (011) rather than (021).

The proposal of an (010) primary slip plane is in agreement with the observations of Connick and May [11] following their original etching examination of surface damage on RDX. It conflicts with the results of Elban and Armstrong [15] who propose a {021} primary slip plane following indentation and etching studies of only the {210} faces. It may be that the secondary slip system noted above will be of this orientation. Further assessments of the anisotropy of hardness on these faces are in course in order to resolve this matter.

4. CONCLUSIONS

The present examination shows, in confirmation of previous work [14] that PETN is a softer solid than RDX. It proves in addition that this distinction can be associated with the relative ease of dislocation slip in the two materials. In the former, microhardness impressions lead to the emission of well-defined slip-traces along (110) and ($1\bar{1}0$) slip planes to a distance of 160 μm (20g load). In the latter, deformation is localised within a much smaller region and along the (010) planes (90 μm, 50g load).

If this proposal is correct, then the distinction in plasticity should be reflected in the properties of the dislocations involved in the process. This study defines accurately the slip planes, the direction and magnitude of the Burgers vectors of the component dislocations can only be assessed by speculation.

For PETN, the slip plane is defined as {110}. The most likely Burgers vectors of pure dislocations which will glide on this plane are [001], <110> and <111> (0.67 nm, 1.32 nm and 1.486 nm respectively). These will have line energies ($E_\ell = kb^2$), where k is the energy factor) of 19, 77 and 103 eV nm^{-1}. The significantly lower energy of the first suggests that the most likely mobile dislocation will be of the type {110} [001]. This energy places PETN in the class of a moderately plastic solid but in which the overall plasticity is limited by the number of potential slip systems.

Of the two slip systems noted for RDX, only the (010) is well-defined. This limits the possible dislocations to those with b[001], [100] and [101] (1.07nm, 1.359nm and 1.690nm respectively). The (010)[001] system is the most likely configuration. Unfortunately no elastic constants are available for this material. The bulk modulus cannot be greatly dissimilar however to that for PETN. Thus the line energy of even the smallest Burgers vector will be considerably greater than that for PETN. Coupled with this, the distortion involved even with a simple [001] vector in a lattice with 8 molecules per unit cell will be considerable and motion of this dislocation will be a complicated and energetic process. The participation of the second slip system and/or motion by partials might facilitate slip. Even then, the reduced energy will still be likely to be much higher than for PETN. The accurate evaluation of such possibilities must await the better and complete definition of the slip systems.

A final question which must be posed relates to the potential involvement of dislocations in the energetic process in these materials. If there is an association, it would be expected to arise from the concentration of mobile dislocations within a microscopic region; their interaction and consequent transfer of energy giving the potential initiating 'hot spot'. Two factors are noteworthy in this context. Firstly, aside from the single rows of pits far from the indentation, the dislocation density around the indentations in PETN is much greater than for RDX. Additionally, although they are mostly inclined to the surface, the dislocations produced by indentations in RDX are not as shallowly inclined as those for PETN. Hence the deformed region in the latter case is confined to a very shallow volume close to the surface. Both factors define that the greater deformation of PETN is confined to a smaller volume than RDX. This concentration could well account for the known greater sensitivity of PETN to impact detonation.

In summary we note that mechanical deformation in PETN proceeds by dislocation motion in the (110) and $(1\bar{1}0)$ slip planes possibly by the motion of {110}[001] type dislocations. In RDX primary slip is limited to the (010) planes and probably involves high energy (010)[001] type dislocations. A secondary ill-defined slip system probably occurs on the (011) or (021) planes. Simple energetic considerations show that the relative hardness of the two materials can be accounted for by the relative energies of the different dislocation slip systems.

ACKNOWLEDGEMENT

We express our grateful thanks to the European Office of the US Army (USARDSG-UK) for their financial support of this work.

REFERENCES

1. F.D. BOWDEN and K. SINGH, Proc. Roy. Soc. (Lond), A227 (1954) 22.
2. W.E. GARNER, ibid, A246 (1938) 203.
3. S.N. HEAVENS and J.E. FIELD, ibid, A338 (1974) 77.
4. R.E. WINTER and J.E. FIELD, ibid, A343 (1975) 339.
5. C.S. COFFEY and R.W. ARMSTRONG, Shock Waves and High Strain Rate Phenomena in Metals: Concepts and Applications, Editors M.A. Meyers and L.E. Muir, Plenum Press, N.Y. 1981.
6. C.S. COFFEY, Phys. Rev., B24 (1981).
7. R.M. HOOPER, B.J. McARDLE, R.S. NARANG and J.N. SHERWOOD, Crystal Growth, Editor B. Pamplin, Pergamon, London (1980), Second Edition p395.
8. P.J. HALFPENNY, K.J. ROBERTS and J.N. SHERWOOD, in preparation.
9. A.D. BOOTH and F.J. LLEWELLYN, J. Chem. Soc., (1947) 837.
10. C.S. CHOI and E. PRINCE, Acta Cryst. B28 (1972) 2857.
11. W. CONNICK and F.G.J. MAY, J. Crystal Growth, 5 (1969) 165.
12. J.J. DICK, J. Appl. Phys., 53 (1982) 6161.
13. P.J. HALFPENNY, K.J. ROBERTS and J.N. SHERWOOD, in preparation.
14. J.T. HAGAN and M.M. CHAUDHRI, J. Materials Sci. 12 (1977) 1055.
15. W. ELBAN and R.W. ARMSTRONG, Seventh International Symposium on Detonation, Annapolis, Maryland, 1981.

Table 1 Summary of Solvent Etching Experiments for PETN

Solvent	Etching Time s	Results
Cyclohexanone	1-20	Hexagonal pits elongated along [001]. Mostly flat-bottomed. Definition poor.
Toluene	5	Surface roughening - no pits.
Ethyl acetate	1	Semi-regular hexagonal pits mostly overetched but some small pits
Other acetate and Proprionate esters	1	No improvement on ethyl acetate
Methyl ethyl ketone	1	As ethyl acetate
Acetone	1	Semi-regular hexagonal pits - sharp and well-defined.
Water	up to 2h	No effect
Acetone/water (various pro-portions)	1	Decreased pit size compared with acetone but poor definition of pits.
Acetic acid	1	No pits - surface roughening only.

CAPTIONS FOR FIGURES

Figure 1 Dislocation etch patterns on (a) and (b), the {110} and (c) the {101} habit faces of PETN crystals. The numbers denote the three types of dislocation etch-pits discussed in the text. (Scale mark 20μm)

Figure 2 Detailed structure of the etch-pits produced by acetone etching of PETN surfaces

a) {110} surface, Type 1 pit, (i) optical micrograph, (ii) interference micrograph, (iii) geometry.

b) {110} surface, Type 2 pit, (i), (ii) and (iii) as above.

c) Geometry of the pits observed on {101} surfaces.

Figure 3 Microhardness impressions (20 g load) on the habit faces of PETN crystals. (Scale mark 20μm)

a) {110} surface b) {101} surface

c) and d) show a) and b) after acetone etching.

Figure 4 Etched microhardness impressions (50g load) on the a) (210), b) (001) and c) (111) habit faces of RDX. (Scale mark 50μm)

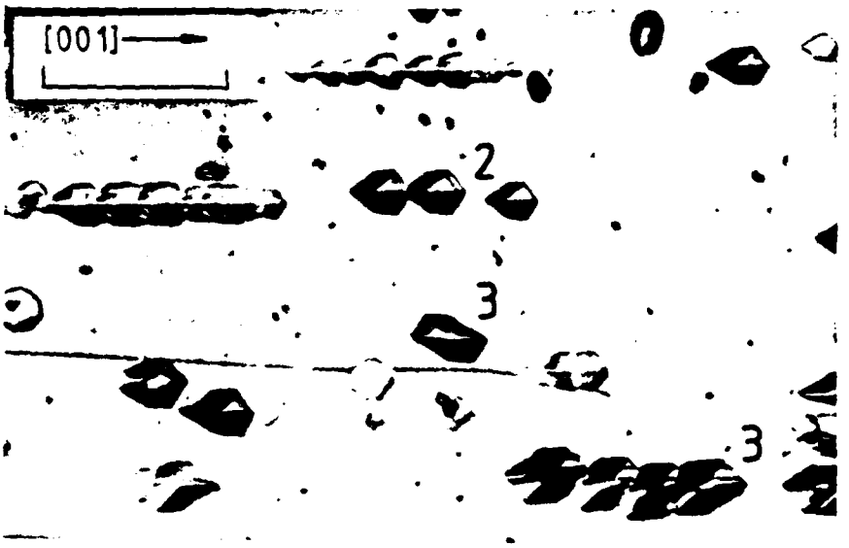

a

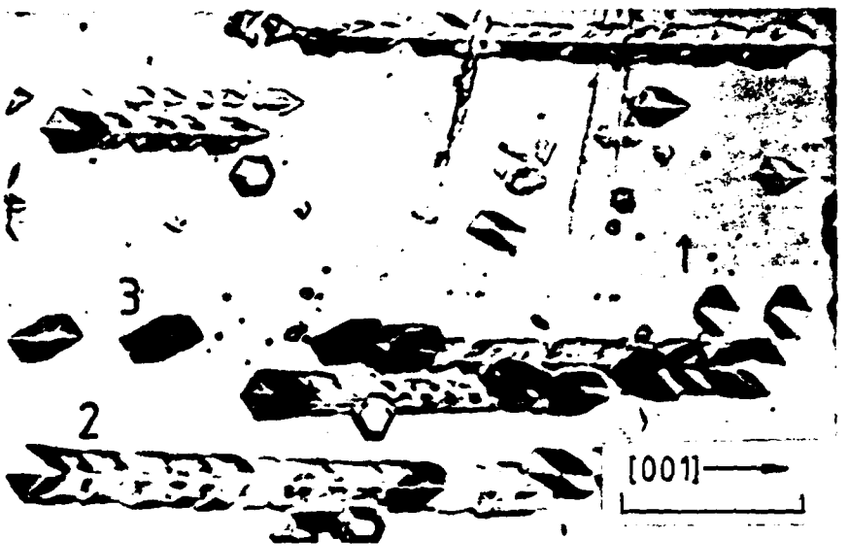

b

c

a(i)

a(ii)

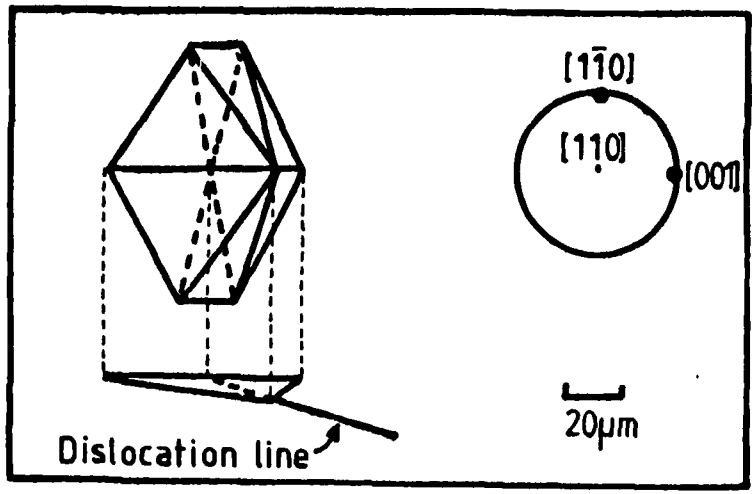

a(iii)

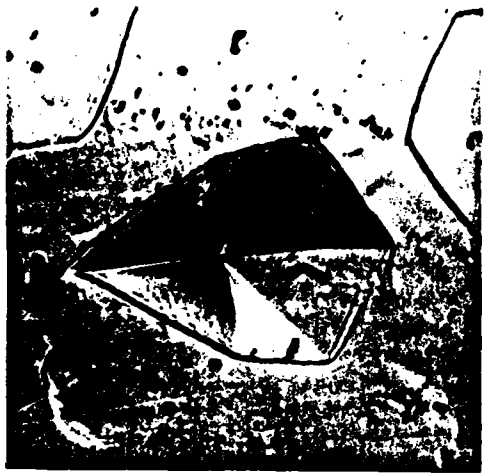

b(i)

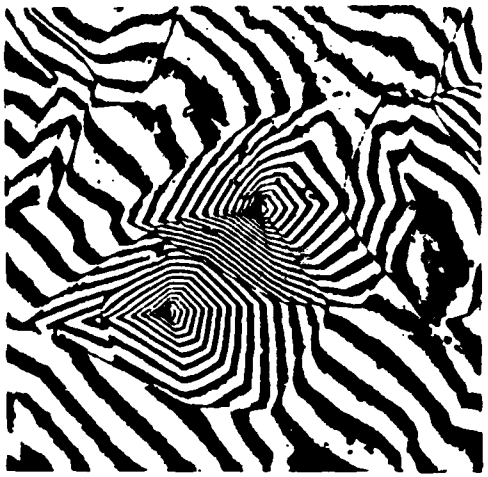

b(ii)

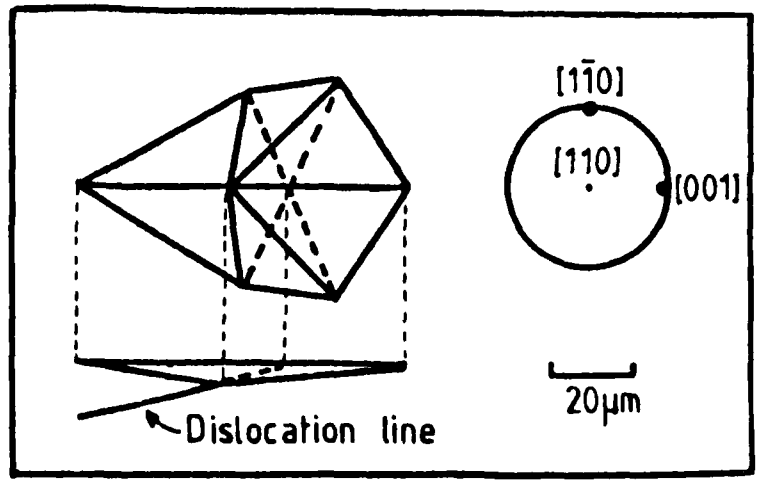

b(iii)

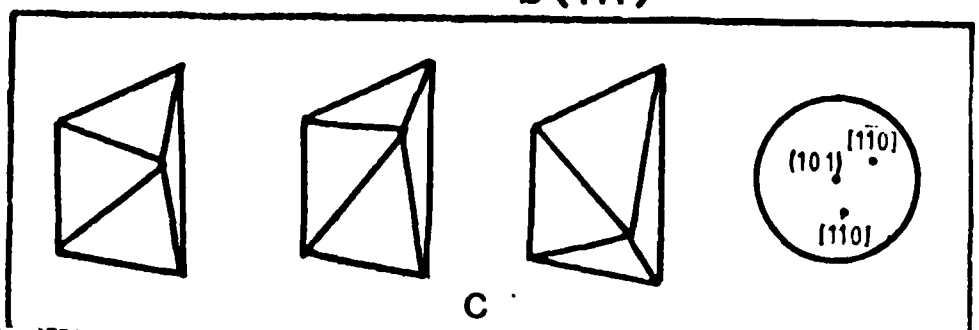

c

FIGURE 2

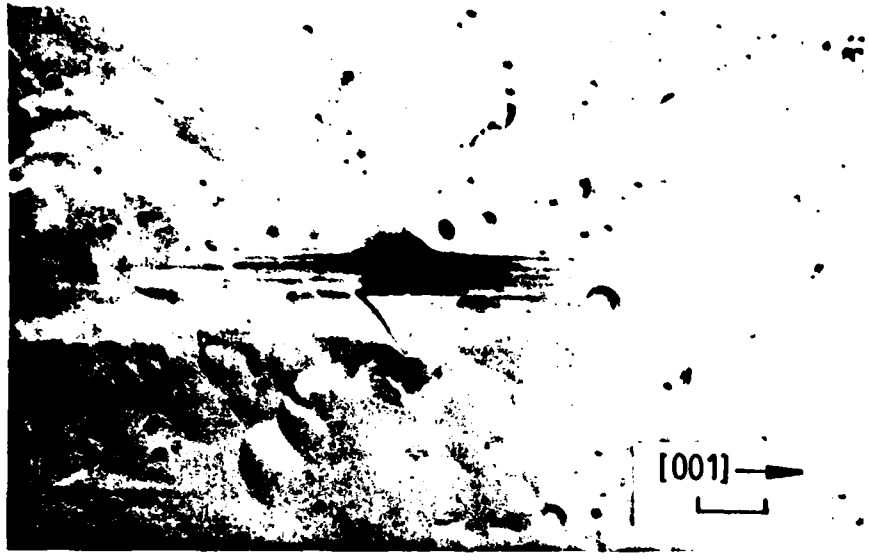

a

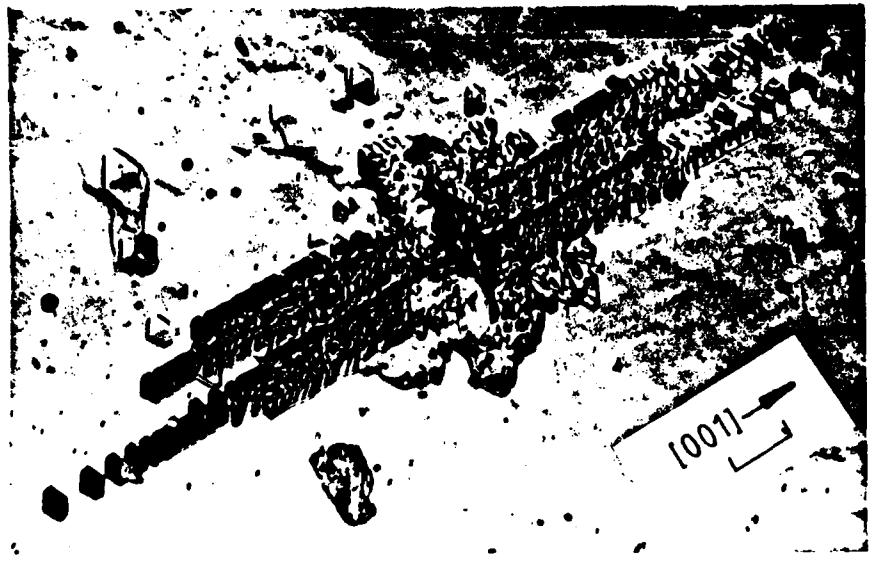

b

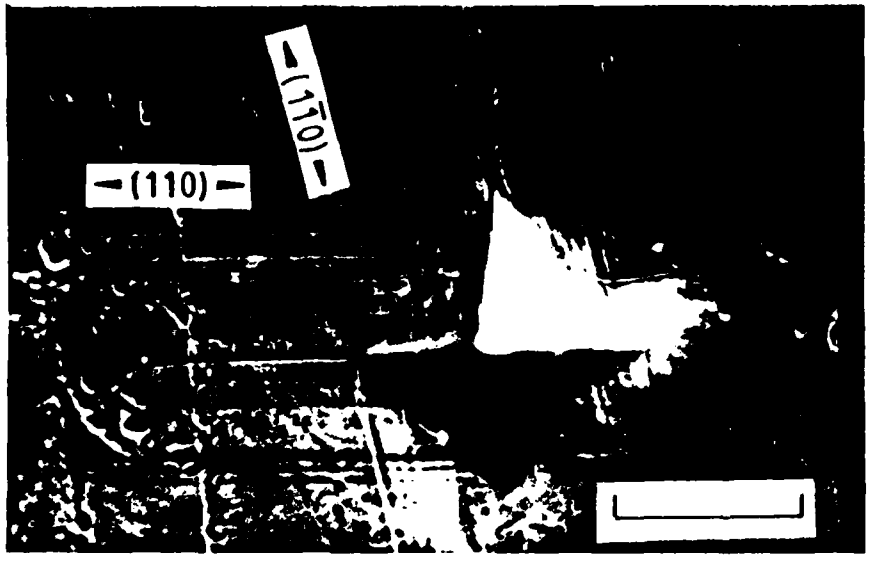

c

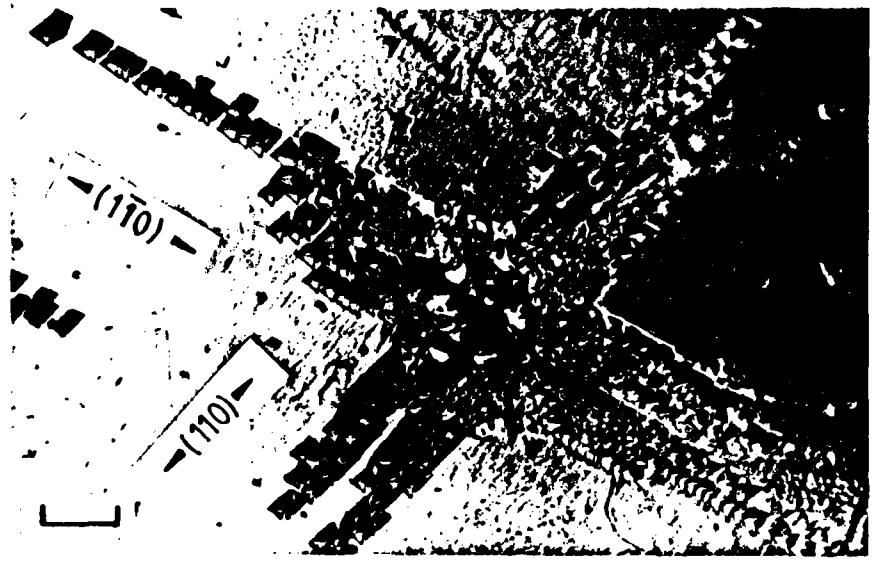

d

FIGURE 3

a

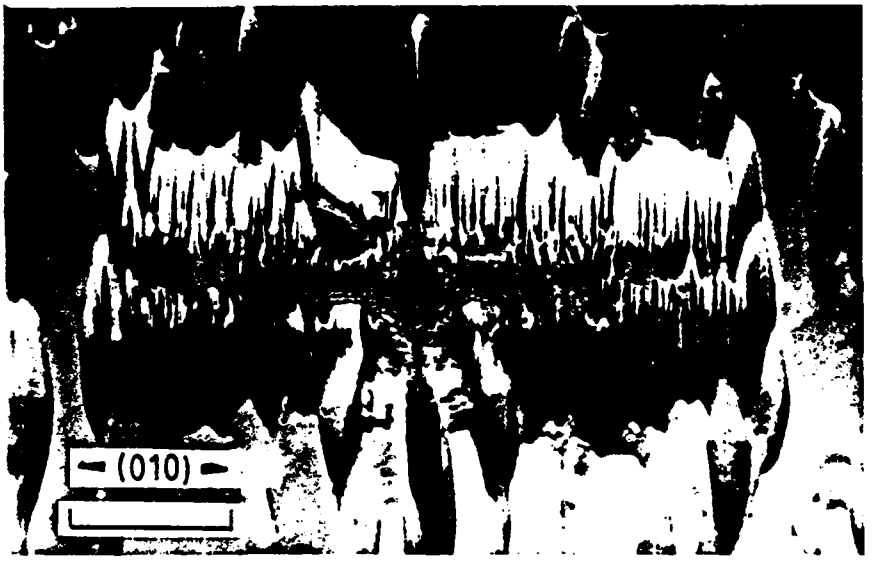

b

c

FIGURE 4

DISLOCATIONS IN ENERGETIC MATERIALS

4. The Crystal Growth and Perfection of Cyclotrimethylene Trinitramine (RDX)

P.J. Halfpenny*, K.J. Roberts and J.N. Sherwood

Department of Pure and Applied Chemistry

University of Strathclyde

Glasgow G1 1XL

Current Address:

*Engineering Materials Laboratories, University of Southampton Highfield, Southampton SO9 5NH

Institut fur Kristallographie, Rhein.-West. Technische Hochschule, Templergraben 55, 5100 Aachen, FRG

ABSTRACT

Large (typically 10 x 15 x 20mm^3) single crystals of cyclotrimethylene trinitramine (RDX) have been prepared from acetone solution by temperature lowering and solvent evaporation techniques. The crystal morphology and perfection are discussed in terms of growth conditions. The basic growth induced defect structure has been revealed by X-ray topography and has been found to comprise dislocations (density 10 to 10^3 lines cm^{-2}) and weakly contrasted growth sector boundaries (typical strain 10^{-5}). Many of the dislocations observed had undergone post-growth motion. The extent of this motion was found to be less in crystals grown more slowly at lower temperatures.

1. INTRODUCTION

The potential importance of lattice defects and crystal perfection in determining the properties and behaviour of solid explosives has been discussed by a number of authors.[1-4] In order to gain a clear understanding of these influences it is necessary to investigate the nature and properties of lattice defects in such materials. The preparation of crystals of varying degrees of perfection is an essential requirement of any such study. This paper describes the growth of single crystals of the important secondary explosive cyclotrimethylene trinitramine (RDX), ranging in quality from highly defective to almost perfect. The perfection of the crystals is assessed by X-ray diffraction topography.

The crystal growth and morphology of RDX has been reported previously by a number of authors. McCrone [5] describes the habits obtained by crystallization of RDX from nitric acid (needles), acetic acid (plates), nitromethane and acetone (massive). Connick and May [6] prepared crystals by temperature lowering of unseeded saturated solutions of RDX in acetone, DMF and cyclohexanone. From acetone and DMF they obtained prismatic crystals exhibiting the forms {210}, {111}, {010}, {100}, {001} and {102} with the first two forms dominant and prism axis [001]. Growth from cyclohexane yielded tablets with {001}dominant. Using the same solvents Koch [7] obtained crystals of RDX up to 80

grammes by the temperature difference method. McDermott and Phakey [8,9] used the temperature lowering method to prepare crystals of RDX from DMF. These crystals were 5 to 10mm in length and up to 5mm thick with {111} faces dominant. Examination by X-ray topography showed them to have very low defect densities.

RDX is a colourless crystalline solid. It crystallizes in the orthorhombic space group Pcba with a = 1.3182nm, b = 1.1574nm, c = 1.0709nm and eight molecules per unit cell.[10] RDX has two known polymorphic forms: RDX I and RDX II.[5] RDX II is very unstable and can be isolated in small quantities and only for a few seconds at the melting point. RDX decomposes thermally at temperatures close to its melting point [11-13]; and photolytically under the influence of UV radiation.[14]

2. CRYSTAL GROWTH

2.1 Growth Conditions

All of the crystals described in this study were grown from supersaturated solutions of RDX in acetone at, or close to ambient temperature. The necessary supersaturation was achieved either by slow cooling or by allowing solvent to evaporate off at constant temperature. The crystal growth apparatus has been described previously.[15] RDX crystals were grown both from seeded solutions and by spontaneous nucleation. In the former case seed crystals were suspended in the growth solution from

fine glass rods or nylon fibre. Polycrystalline RDX (99.5% purity), obtained from PERME, Waltham Abbey, was purified by multiple recrystallization from distilled acetone. The solubility (S) of RDX in acetone [16] is 12g per 100g of solvent (313K) with a solubility ratio, (dS/dT)/S, of 0.025 K^{-1}. These parameters lie within the ranges previously found to be suitable for the growth of high quality single crystals from solution.[15] Crystals were grown by temperature lowering at rates of between 0.005 and 0.02 Khr^{-1} in the temperature range 317 to 298K. Growth by solvent evaporation was carried out in the crystallizers both at room temperature and below. Small crystals (up to 0.5cm^3) were also grown by spontaneous nucleation in evaporating dishes at room temperature. The specific growth conditions of crystals prepared in the crystallizers are shown in Table 1.

2.2 Morphology

The crystals shown in Figure 1 were prepared by solvent evaporation and were nucleated spontaneously on the bottom of an evaporating dish at room temperature. These examples were all obtained from the same growth solution and illustrate the variations in morphology which were observed under such growth conditions. Of the three habit types, equant crystals (A) were dominant. These exhibited the forms {001}, {111} and {210}. In addition, prismatic crystals (B) with {210} faces predominating were frequently observed. The {001} tablets (C) which also exhibited {210} facets, were relatively rare, comprising less

than 10% of the crystals from any growth solution. It is noteworthy that few crystals of the equant habit larger than a few millimeters were observed. Amongst the larger crystals the prismatic habit dominated.

In contrast, crystals grown from seeds in the crystallizers exhibited only minor variations in morphology. This was true of both the slow cooling and solvent evaporation techniques. All of these crystals were of the prismatic habit with {210} dominant and {111} secondary in facial area. The relative facial area of the {210} form was found to increase with decreasing growth rate, resulting in a more pronounced elongation along the prism axis. The small {100} and {010} faces were absent in the more slowly grown crystals. Figure 2 shows a typical crystal of RDX prepared by seeded growth in a crystallizer. The morphologies and dimensions of all similarly prepared crystals are included in Table 1.

3. CRYSTAL PERFECTION

3.1 X-Ray Topography

As-grown crystals of RDX were sectioned using a solvent saw. The resulting slices were polished on a soft, solvent soaked cloth and were then lightly etched to remove any preparation-induced surface damage. The most suitable solvents for slicing and

polishing were found to be dimethyl formamide and cyclohexanone respectively. Two different slice planes were employed, namely (001) and (010).

By use of these slice planes a large selection of useful reflections were made available. Transmission X-ray topographs were recorded using the conventional Lang technique.[17] Copper Kα radiation was used throughout. For this wavelength the linear absorption coefficient of RDX is 1.548×10^3 m^{-1}. Samples were typically 1mm in thickness giving a value of $\mu t = 1.5$.

3.2 Survey of Growth Induced Defects

a) Growth Sector Boundaries

The visibility of growth sector boundaries in X-ray topographs depends upon the strain associated with the boundary and upon the strain sensitivity of the reflection used. Many of the topographs of RDX showed no images of growth sector boundaries and those which did showed only weakly contrasted images of these defects. Figures 3 and 4 show 200 and 021 topographs of an RDX crystal slice. The former reflection has a relatively low strain sensitivity (intrinsic rocking curve width $\Delta\theta = 1.09$ arc seconds) and thus yields dislocation images of high spatial resolution. No images of growth sector boundaries are visible. The locations of boundaries are, however, indicated by the points at which growth dislocations undergo abrupt changes in line directions upon passing from one growth sector to another (e.g. at point A in Figure 3). In the more strain sensitive 021 reflection ($\Delta\theta$ =

0.73 arc seconds) the growth sector boundaries are clearly visible. The strain sensitivity (R) of a reflection can be obtained by differentiation of Bragg's Law:

$$R = \Delta d/d = -\Delta\theta/\mathrm{Tan}\ \theta$$

where d is the lattice spacing and θ is the Bragg angle. Thus we obtain $R(200) = 2.25 \times 10^{-5}$ and $R(021) = 1.15 \times 10^{-5}$. These values therefore define the strain associated with growth sector boundaries in RDX.

b) Inclusions

Gross [17], using optical microscopy, reported net-like arrays of solvent inclusions in crystals of RDX. In this study X-ray topographs revealed no such arrays. Solvent inclusions were generally few in number. This is most probab'y due to the accurate control of growth conditions employed in this study.

c) Dislocations

Dislocation densities in RDX crystals were found to be in the range 10 to 10^3 cm^{-2}. The most striking feature of these dislocations is that few of them are straight (see Figure 5). Configurations such as these are indicative of either mechanically introduced dislocations or of growth induced dislocations which have undergone post-growth motion by glide or climb. Examination of the topographs reveals that many of the dislocations propagate in the general direction from crystal

centre to the crystal faces. In addition many of them (see those labelled A in Figure 5) undergo sharp changes in line direction upon crossing a growth sector boundary. These features confirm that the dislocations are growth induced and have undergone post-growth motion. The origins and character of dislocations in RDX, together with the nature of the observed post-growth motion are discussed in detail elsewhere.[19,20]

3.3 The Influence of Crystal Growth Conditions upon Crystal Perfection

The topographs shown in Figures 3, 5 and 6 illustrate the variation in perfection of RDX crystals grown under different conditions. Figure 6 shows a crystal grown from acetone solution by rapid solvent evaporation. The crystal is so defective that resolution of individual defects is impossible. Growth from a seeded solution by temperature lowering yielded crystals of much higher perfection as shown by the topograph in Figure 5. The crystal from which this slice was taken was grown from acetone at a cooling rate of $0.02Khr^{-1}$ over the temperature range 317K to 308K. The Pendellosung fringes visible at the edges of the sample indicate a high degree of crystal perfection. Figure 3 shows a topograph of another crystal slice grown by temperature lowering. In this case the cooling rate was much slower ($0.01Khr^{-1}$) and the growth temperature somewhat lower (305 to 302K). A marked increase in crystal perfection is evident. It

is also noteworthy that the dislocations in this sample have undergone less motion than those in the crystal grown more rapidly at a higher temperature.

Figure 7 shows two further slices cut from the same crystal as that shown in Figure 3. Each slice is progressively further from the centre of the crystal. A marked decrease in dislocation density is found as the distance from the centre of the crystal increases. This results in an almost defect-free slice taken from the very edge of the crystal (Figure 7b).

4. DISCUSSION

4.1 Morphology

The Law of Donnay and Harker [21] provides a good indication of the relative morphological importance of crystal forms, namely that the morphological importance decreases with increasing reticular area. The reticular areas and interplanar spacings for low indexed planes of RDX are listed in Table 2. As a consequence of the near equality of the unit cell dimensions and the dense packing of molecules in the unit cell ($Z = 8$) there is little difference between these parameters. The large number of crystallographic forms is a direct result of this. A second consequence is that factors such as solute-solvent interactions and growth conditions have a more pronounced effect on crystal

morphology. Hence the variations in morphology of crystals grown from different solvents observed by previous workers, and the variations with other growth conditions observed in this study.

The largest variations in morphology were observed amongst crystals grown by solvent evaporation in dishes. The fact that all three morphologies were obtained from any given growth solution indicates that impurity effects and growth temperature were not responsible for the differences. The observed variations in dish grown crystals are attributed to local variations in supersaturation. For example a region of low supersaturation will occur close to a cluster of growing crystals while an isolated crystal will be subjected to a considerably higher supersaturation. Another possible cause of the differences in morphology is different defect structures of the seed crystals. However the fact that seed crystals of the equant habit yielded prismatic crystals by temperature lowering suggests that this is not the case.

In view of the relatively narrow range of growth conditions imposed upon crystals prepared by temperature lowering only minor variations in morphology are to be expected. The increasing dominance of {210} faces with decreasing growth rate indicates this form is favoured by conditions of low supersaturation. The converse is true of the forms {100} and {010} which disappear with decreasing growth rate. This suggests that under conditions

of high supersaturation (rapid temperature lowering rate) the equant habit will predominate. This hypothesis was not investigated however.

4.2 Crystal Perfection

The greater perfection of crystals grown by temperature lowering is due primarily to the accurate control of growth conditions which this technique allows. Such control minimises solvent incorporation which arises from large fluctuations in growth rate. Hence the absence of growth banding and the low incidence of solvent inclusions in crystals grown in this way. Since solvent inclusions are the major cause of growth dislocations, the reduction in the number of those also brings about a decrease in dislocation density.

The strain associated with growth sector boundaries in RDX is relatively small in comparison with similar materials.[22] This fact is a direct result of the similarity in the reticular areas of the lower index planes discussed above. The small differences in reticular areas of the observed forms implies a corresponding similarity in the growth rates. A large disparity in the growth rates of two forms would result in highly strained growth sector boundaries between the two and a greater tendency for solvent incorporation at the boundary. The converse is true and is the case in crystals of RDX.

5. CONCLUSIONS

In summary, crystals of RDX were grown from acetone solution by temperature lowering and by solvent evaporation. In the case of unseeded growth by solvent evaporation, three distinct habits were observed: Prismatic, equant and tabular. Crystals grown from seeds exhibited the prismatic habit only with the forms {210}, {111}, {001}, {010}, {100} and {102}.

The crystal perfection improved with slower growth rates and lower growth temperatures. Dislocation densities were in the range 10 to 10^3 cm^{-2}, the former being typical of crystals grown slowly by temperature lowering. The observed dislocation motion was also found to be less extensive at slower growth rates and lower temperatures. The strain associated with growth sector boundaries in RDX crystals has been estimated at $\sim 10^{-5}$.

REFERENCES

1. F.P. Bowden, 1958, Proc. Roy. Soc. A246, 146.
2. W.L. Elban and R.W. Armstrong, 1981, 7th International Symposium on Detonation.
3. J.S. Jach, 1962, Nature 196, 827.
4. K. Singh, 1956, Trans. Farad. Soc. 52, 1623.
5. W.C. McCrone, 1950, Anal. Chem. 22, 954.
6. W. Connick and F.C. May, 1969, J. Cryst. Growth 5, 65.
7. E.W. Koch, Einfuehrungssymp. Inst. Chem. Tech. Unters 1973, 478.
8. I.T. McDermott and P.P. Phakey, 1971a, Phys. Stat. Sol. (a) 8, 505.
9. I.T. McDermott and P.P. Phakey, 1971b, J. Appl. Cryst. 4, 479.
10. C.S. Choi and E. Prince, 1972, Acta Cryst. B28, 2857.
11. J.J. Batten and D.C. Murdie, 1970, Aust. J. Chem. 23, 73.
12. J.J. Batten, 1971, Aust. J. Chem. 24, 945.
    ibid. 24, 2025.
13. J.J. Batten, 1972, Aust. J. Chem. 25, 2337.
14. J. Stals, A.S. Buchanan and C.G. Barraclough, 1971, Trans. Farad. Soc. 67, 1739.

15. R.M. Hooper, B.J. McArdle, R.S. Narang and J.N. Sherwood, 1980, In "Crystal Growth" (Ed. B. Pamplin) Pergamon, London, 2nd Edition, p395.

16. M.E. Sitzmann and S.C. Foti, 1975, J. Chem. Eng. Data 20, 53.

17. A.R. Lang, 1978, "Diffraction and Imaging Techniques in Materials Science", (Ed. Amelinckx et al.) p623.

18. K. Gross, 1970, J. Cryst. Growth 6, 210.

19. P.J. Halfpenny, 1982, PhD Thesis, University of Strathclyde.

20. P.J. Halfpenny, K.J. Roberts and J.N. Sherwood, 1983a, Publication in preparation.

21. J.D.H. Donnay and D. Harker, 1937, Amer. Miner. 22, 446.

22. P.J. Halfpenny, K.J. Roberts and J.N. Sherwood, 1983b, submitted to J. Cryst. Growth.

FIGURE CAPTIONS

Figure 1 RDX crystals grown in dishes by solvent evaporation showing equant (A), prismatic (B) and tabular (C) habits. (Scale mark 1mm).

Figure 2 Typical crystal of RDX grown from seeded acetone solution by temperature lowering. (Scale mark 1cm).

Figure 3 200 topograph of an RDX slice cut from a crystal grown at $0.01 Khr^{-1}$. (Scale mark 1mm).

Figure 4 021 topograph of an RDX crystal slice showing growth sector boundaries. (Scale mark 1mm).

Figure 5 420 topograph of a slice cut from a crystal grown by temperature lowering at $0.02 Khr^{-1}$. (Scale mark 1mm).

Figure 6 200 topograph of an RDX crystal grown by rapid solvent evaporation. (Scale mark 1mm).

Figure 7 $\bar{4}20$ topographs of slices cut from the same crystal as that shown in Figure 3. (Scale mark 1mm).

Crystal	Stirring RPM	Growth* Method	Average Rate Khr^{-1}	Temp Range K	Forms						Dimensions		
					{210}	{111}	{001}	{010}	{100}	{102}	[001]	[010]	[100]
1	-	E	-	~298	✓	✓	✓	✓	✓	✓	12	9	4
2	60	C	0.016	317 308	✓	✓	✓	✓	-	✓	21	15	10
3	60	E	-	~298	✓	✓	✓	✓	✓	✓	15	12	6
4	60	C	0.020	315 305	✓	✓	✓	✓	✓	✓	23	15	10
5	60	C	0.010	305 302	✓	✓	✓	✓	-	✓	20	15	10
6	60	C	0.010	304 297	✓	✓	✓	✓	-	✓	13	9	6
7	60	C	0.010	303 298	✓	✓	✓	✓	✓	✓	19	12	8
8	20	E	-	303	✓	✓	✓	✓	✓	✓	28	23	13
9	10	C	0.005	304 298	✓	✓	✓	-	-	✓	23	13	8
10	60	E	-	290	✓	✓	✓	✓	-	✓	19	12	7

*Growth method E = solvent evaporation; C = slow cooling

TABLE 1

RDX CRYSTALS GROWN FROM ACETONE SOLUTION

No	Form	Reticular Area (mesh area) (s/b^2)	Interplanar spacing (nm)
1	{111}	1.807	0.675
2	{200}	1.851	0.659
3	{020}	2.109	0.579
4	{210}	2.131	0.573
5	{002}	2.228	0.536
6	{021}	2.397	0.509
7	{211}	2.416	0.505
8	{102}	2.459	0.496

TABLE 2

RDX RETICULAR (MESH) AREAS AND

INTERPLANAR SPACINGS

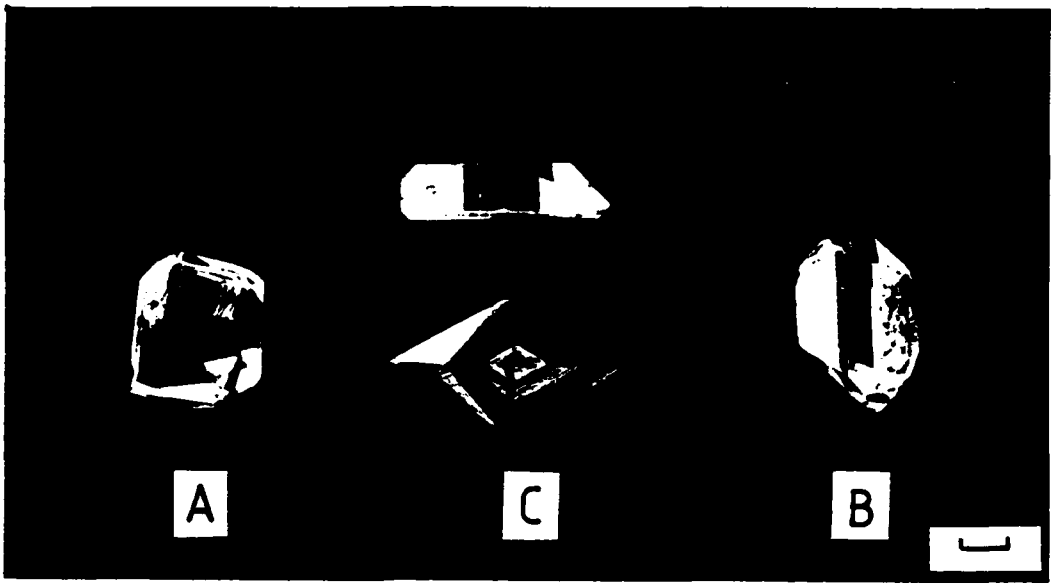

FIGURE 1

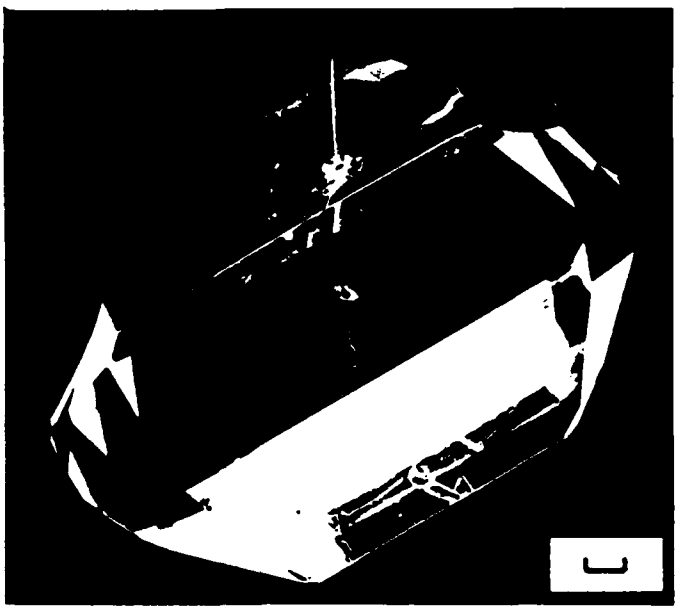

FIGURE 2

FIGURE 3

FIGURE 4

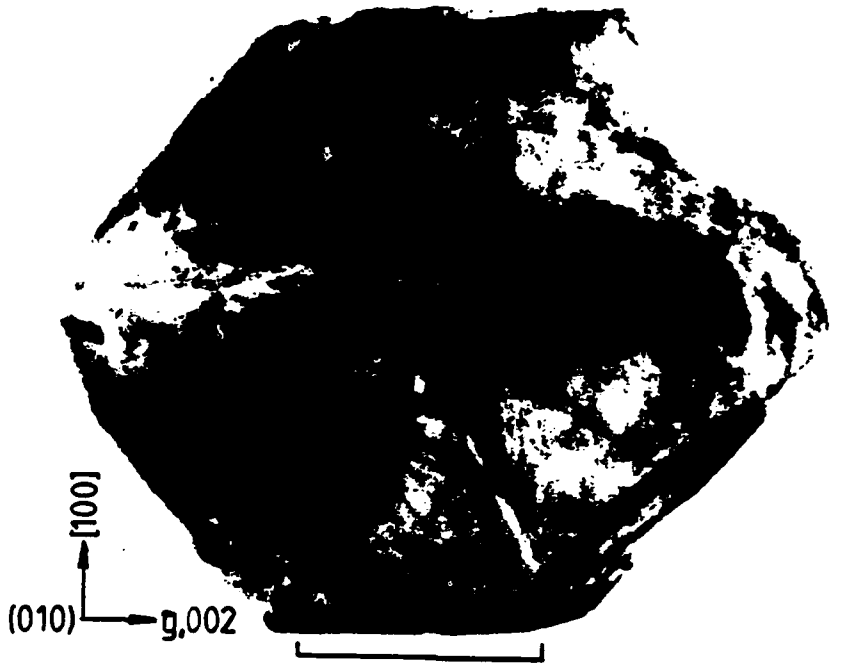

FIGURE 6

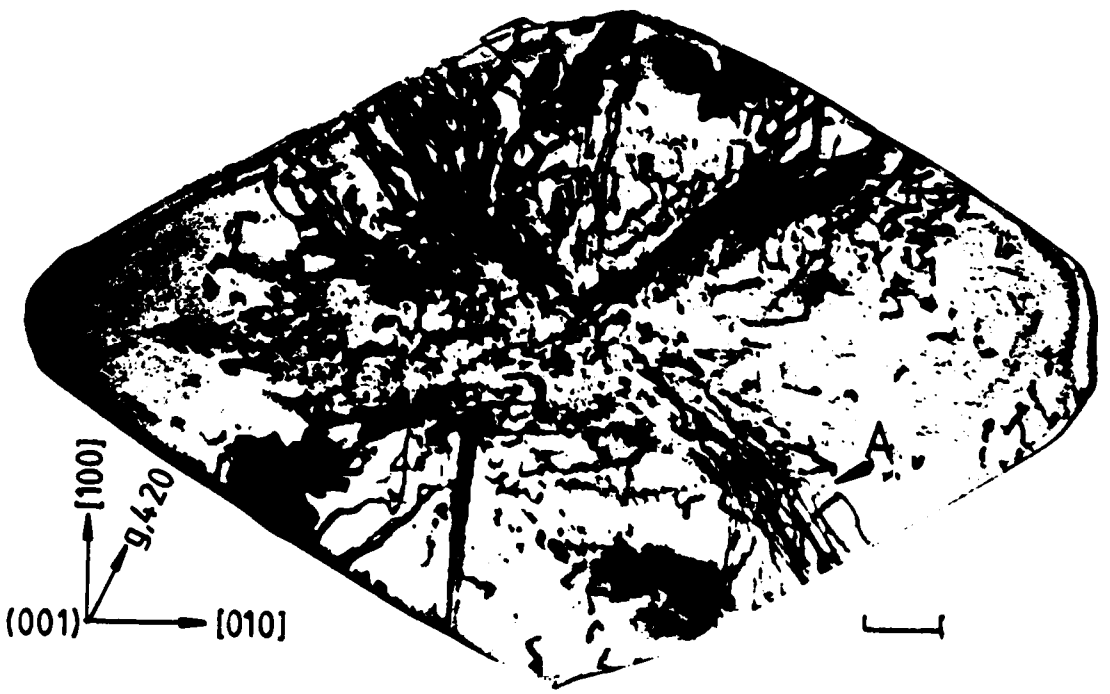

FIGURE 5

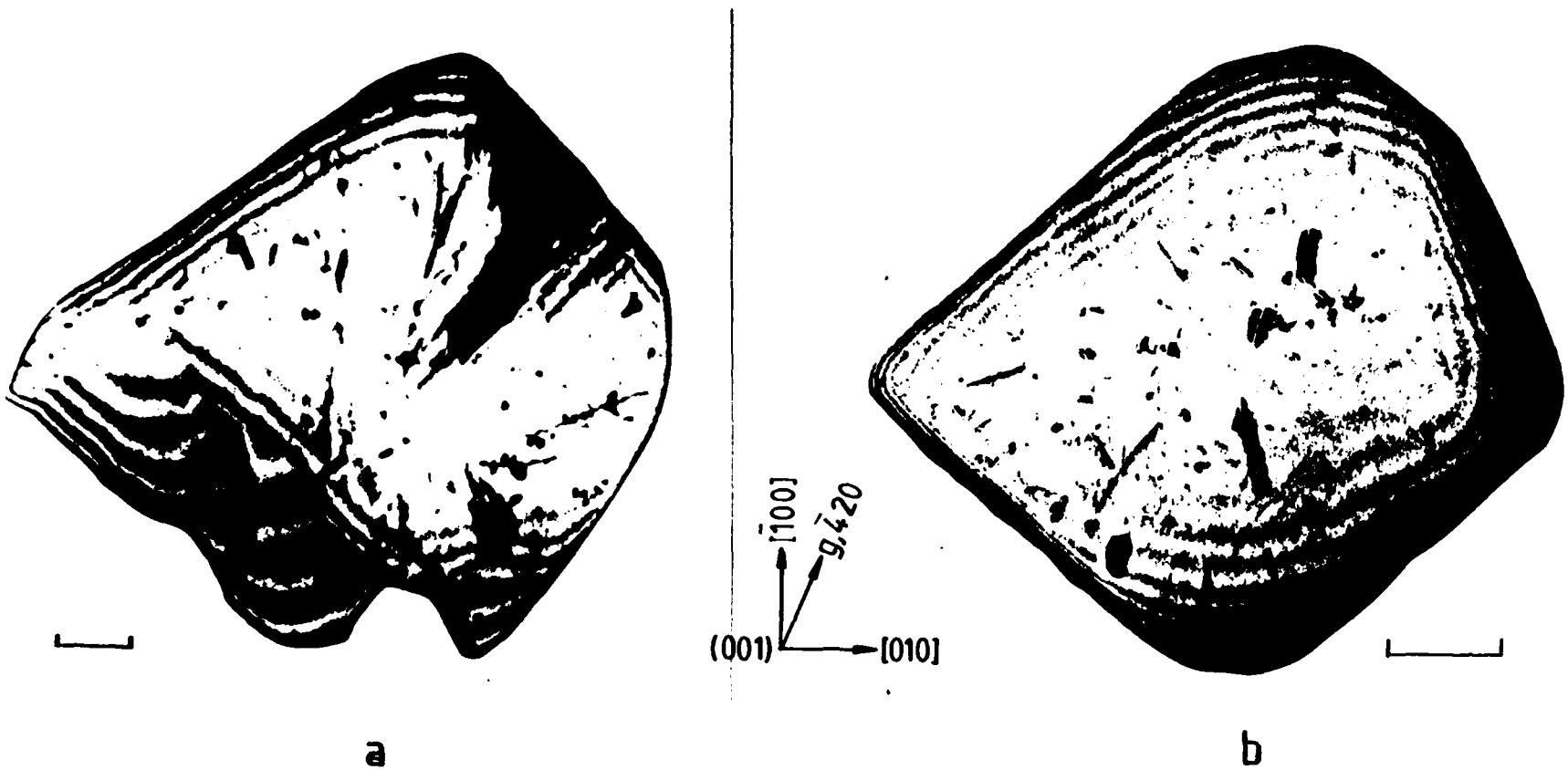

a

b

FIGURE 7

DISLOCATIONS IN ENERGETIC MATERIALS

5. Dislocation Characterization and Post Growth Motion in Single Crystals of Cyclotrimethylene Trinitramine

P J Halfpenny*, K J Roberts and J N Sherwood

Department of Pure and Applied Chemistry

University of Strathclyde

Glasgow G1 1XL

*Present Address:

Engineering Materials Laboratories

University of Southampton

Southampton SO9 5NH

United Kingdom

ABSTRACT

Dislocations in solution-grown crystals of cyclotrimethylene trinitramine (RDX) have been observed and characterized by transmission X-ray topography. The dislocations were found to have the following Burger's vectors: [001], [010], [100], <011> and <110>. With the exception of one pure edge dislocation type they were all of mixed character. A few of the dislocations were straight and showed characteristics typical of growth induced dislocations. Most, however, exhibited irregular line directions indicative of post-growth motion. In addition, a number of narrow dislocation helices were observed. The observed dislocation configurations are discussed in terms of climb, cross-slip and combined climb/slip mechanisms. Evidence is presented for the existence of an alternative (001) slip plane additional to the (010) plane previously defined by microhardness indentation.

1. INTRODUCTION

The physical and chemical properties of solid explosives, as with any other crystalline solid, are greatly influenced by the number and properties of crystal defects within the materials. This has been well demonstrated in the case of the chemical reactivity of explosives (Singh 1956, Jach 1962) and many other materials (Thomas 1969, Meyer 1978, Herley and Levy 1972). It has also been suggested that processes associated with the formation and migration of lattice defects are fundamentally involved in the impact initiation of explosives (Bowden 1958, Afanasev and Bobolev 1971, Winter and Field 1975, Coffey 1981, Coffey and Armstrong 1981, Elban and Armstrong 1981, Field, Swallow and Heavens 1982). Despite the potential importance of crystal defects in influencing the behaviour of solid explosives, very little is known of the nature and properties of lattice defects in such materials.

This study describes the characterization of dislocations in solution-grown crystals of the secondary organic explosive cyclotrimethylene trinitramine (RDX). The origins of the dislocations are discussed. Possible mechanisms which could give rise to the observed dislocation configurations are proposed.

Several studies of defects in RDX crystals have been reported. Gross (1970) studied solvent inclusions in RDX crystals using optical microscopy. Connick and May (1969) used etching to reveal dislocations and to investigate plastic deformation and dislocation polygonisation by heating. McDermott and Phakey (1971 a, b) and Lang (1962) investigated defects in RDX crystals using X-ray topography. Of these studies, only that of McDermott and Phakey provided any information on the character of the dislocations. This was, however, rather limited and contained no detailed characterization of dislocation configurations.

2. SAMPLE PREPARATION

Single crystals of RDX were prepared by seeded growth from saturated acetone solution using temperature lowering and solvent evaporation techniques at, or close to, ambient temperature (290 - 317K). The crystals were of a prismatic habit, typically $10x15x20mm^3$ and exhibited the forms {210}, {111}, {001}, {100} and {102}, with the former two dominant. The prism axis was [001]. The growth, morphology and perfection of RDX crystals is discussed in detail elsewhere (Halfpenny 1982; Halfpenny, Roberts and Sherwood 1984a).

The crystals were sectioned for X-ray topography, parallel to either (001) or (010), using a solvent saw. The resulting slices were polished on a soft, solvent soaked, cloth and then subjected to a free etch. The most suitable solvents were found to be dimethyl formamide (DMF) for sectioning, and cyclohexanone for both the polish and free etch.

3. ANALYSIS OF POSSIBLE DISLOCATION TYPES

In characterizing dislocations in RDX, it is valuable to consider the possible dislocation types which may exist in this material.

3.1 Burger's Vectors

RDX crystallizes in the orthorhombic space group Pbca with a = 1.3182nm, b = 1.1574nm, c = 1.0709nm and eight molecules per unit cell (Choi and Prince 1972). The dominant component of the energy of a dislocation (the elastic line energy) is proportional to the square of the magnitude of the Burger's vector. Consequently, the shorter lattice translations are favoured as dislocation Burger's vectors. Since the RDX unit cell is primitive, there is no halving of lattice translations due to centring and the Burger's vector lengths increase in the sequence shown in table 1. While not discounted, dislocations with Burger's vectors longer than <111> were considered improbable for energetic reasons.

3.2 Growth Induced Dislocations

Growth induced dislocations are generally straight and tend to lie along a number of discrete, well-defined, line directions. These preferred directions are characteristic of the Burger's vector $\underline{b}$ and the growth direction $\underline{n}$, and correspond to the direction along which the energy per unit length of the dislocation is a minimum (Klapper 1972). Thus the line directions of growth induced dislocations can be predicted by determining these directions of minimum energy (Klapper 1972, 1973, 1974). Although the elastic constants required for such calculations are unavailable in the case of RDX, much valuable information can be deduced from the following general observations (Klapper 1980):-

i) For a pure screw dislocation the line direction, $\underline{l}$, is parallel to $\underline{n}$.

ii) For a pure edge dislocation $\underline{l}$ is also parallel to $\underline{n}$ provided the latter is parallel to a twofold symmetry axis.

iii) The line direction of a mixed dislocation lies between, and is usually coplanar with, $\underline{b}$ and $\underline{n}$.

Each combination of a Burger's vector and a growth direction defines a possible growth dislocation line direction. By considering all combinations of $\underline{b}$ and $\underline{n}$, the possible growth dislocation families can be deduced. Table 2 lists the dislocation families which could occur in the dominant {210} and {111} growth sectors of RDX together with deductions about their possible line directions.

3.3 Mechanically Induced Dislocations

Studies of microhardness indentation and etching (Halfpenny, Roberts and Sherwood 1984b) have defined the active slip plane in RDX to be (010). There are also indications of a possible secondary slip plane which could be either {021} or {011}. Since the Burger's vector of a mechanically induced dislocation must lie in the slip plane, the only possible Burger's vector for such dislocations are [100], [001] or <101>. <011> is also possible if a secondary slip plane {011} does indeed exist.

4. CHARACTERIZATION

Transmission X-ray topographs were recorded using the Lang technique (Lang 1978), with CuK_α radiation. For this wavelength the linear absorption coefficient, μ, of RDX is $1.548 \times 10^{-3} m^{-1}$. Thus with typical slice thicknesses, t = 1mm, the product, μt, was approximately 1.5. Images were recorded on Agfa Structurix D4 X-ray film.

A selection of RDX crystals grown from acetone by slow cooling was examined by X-ray topography. The dislocations were characterized by contrast variations using the invisibility condition $\underline{g}.\underline{b} = 0$. While this condition strictly only applies to the invisibility of a pure screw dislocation, it is the component of strain parallel to $\underline{b}$ which dominates in both edge and mixed dislocations. Thus complete or near-invisibility of such dislocations is frequently obtained when the condition $\underline{g}.\underline{b} = 0$ is satisfied. This was indeed the case for most of the dislocations observed in this study.

Table 3 summarizes the predominant dislocation types observed and characterized in crystals of RDX. Two slices have been selected to illustrate these types and their characterization. The first of these samples is shown schematically in Figure 1. Figure 2 shows X-ray topographs taken using the following reflections: 200, 102, 002, $4\bar{2}0$, $0\bar{2}3$ and $2\bar{2}0$. The slice plane orientation is (010). Four growth sectors, corresponding to the (210), $(\bar{2}10)$, (111) and (010) faces, are present in this slice.

4.1 Dislocations with Burger's Vector [001]

The dislocations labelled A and B in Figure 1 are invisible in the 200, $4\bar{2}0$ and $2\bar{2}0$ reflections. Their Burger's vectors are therefore uniquely defined as [001]. Those labelled A are straight and, within the errors of measurement, lie parallel to the $\{210\}$ growth normals. These observations show these dislocations to be growth induced and to be pure edge in character. Those labelled B, lying in the (111) growth sector, are of mixed character and exhibit markedly different configurations to those labelled A. Although they follow irregular paths,their overall line directions are parallel and propagate from crystal centre to crystal face. They are, therefore, also growth induced dislocations but for most of their length have undergone post-growth motion.

4.2 Dislocations with Burger's Vector [100]

The dislocations labelled C in Figure 1 are invisible in both the 002 and the $0\bar{2}3$ reflections. The only Burger's vector which satisfies the condition $\underline{g}.\underline{b} = 0$ for both these reflections is [100]. The dislocations are present in both of the $\{210\}$ growth sectors. They can be seen most clearly in the 200 reflection in which many of the superimposed dislocations are invisible. Although these dislocations show large deviations from linearity, several factors indicate that they are growth induced. Firstly, several dislocations appear to originate from a solvent inclusion (I) and, secondly, they propagate close to the $\{210\}$ growth normals for much of their length. We therefore conclude that these dislocations are growth induced and have undergone some form of post-growth motion.

4.3 Dislocations with Burger's Vector <110>

The dislocations labelled D are invisible in the 002 reflection only. This information limits the possible Burger's vectors to [010], [100] and <110>. The dislocations are strongly contrasted in the 200 reflection which suggests that [010] is not the Burger's vector. They are also visible in the 023 reflection. Previously characterized dislocations with $\underline{b}$ [100] are invisible in this reflection which indicates that [100] is not the Burger's vector of dislocations D. By a process of elimination they are therefore characterized as <110> Burger's vector dislocations. They cannot be seen in the $2\bar{2}0$ reflection but because of image distortion and superimposition of defects it is not possible to determine whether or not they have indeed disappeared. If they have, this would confirm the Burger's vector assignment as [110]. The origin of these dislocations is not clear and is considered further in section 5.

4.4 Dislocations with Burger's Vector <011>

Only one dislocation with this Burger's vector is visible in this slice. It is labelled E and becomes invisible in the 200 reflection only. Three Burger's vectors are consistent with this observation, namely [001], [010] and <011>. Dislocation E remains strongly contrasted in the $4\bar{2}0$ and $2\bar{2}0$ reflections, while those previously characterized as $\underline{b}$ [001] become invisible. We therefore conclude that [001] is not the Burger's vector of dislocation E. Similarly, it is strongly contrasted in the 102

and 002 reflections. A Burger's vector of [010] is therefore also unlikely. The weight of evidence thus indicates the Burger's vector of dislocation E to be <011>. The specific Burger's vector, however, cannot be determined from the information available. The dislocation undergoes an abrupt change in line direction as it crosses a growth sector boundary but is otherwise straight. This behaviour is typical of growth induced dislocations.

4.5 Dislocations with Burger's Vector [010]

The second sample is a (001) slice which is shown schematically in Figure 3. Figure 4 shows topograhs taken using 200 and 040 reflections. In addition to many of the Burger's vectors observed in the first example, this slice also contains dislocations with Burger's vector [010]. These dislocations, labelled F in Figure 3, are invisible in the 200 reflection. This limits the possible Burger's vectors to [001], [010] or <011>. The dislocations are strongly contrasted in both the 040 and 420 (not shown) reflections. This suggests that [001] is not the Burger's vector. The dislocations of Burger's vector <011> characterized previously were straight while those in the present example exhibit irregular line directions. This marked difference in behaviour suggests that they do not have the same Burger's vector since, as will be discussed later, there is a strong correlation between dislocation character and post-growth motion. This process of elimination strongly suggests the Burger's vector to be [010].

5. DISCUSSION

The dislocations observed in crystals of RDX show considerable variety both in their Burger's vectors and in the configurations they adopt. The observed dislocation types were found to be of mixed character with one exception, namely the pure edge dislocations with $\underline{b}$ [001] in the {210} sectors. It will be recalled that this dominance of mixed character amongst growth dislocations was predicted by examination of possible Burger's vectors and growth directions.

It is noteworthy that, while the shorter length Burger's vectors predominate, some high energy Burger's vectors such as <110> and <011> also occur. Similar situations have been reported for growth dislocations in other materials such as pentaerythritol tetranitrate (Halfpenny, Roberts and Sherwood 1984c) and ammonium dihydrogen orthophosphate (Bhat, Roberts and Sherwood 1983). In some cases the longer Burger's vectors can even predominate. These observations lead us to suggest that, up to some critical value, the line energy of a growth dislocation is not the major factor in determining whether or not a particular Burger's vector occurs. Bearing in mind the manner in which growth dislocations are formed, a more significant factor may be the nature of the misorientation from which the dislocation originates.

5.1 Dislocation Configurations

The dislocation configurations observed in RDX fall into three categories:-

1) Straight growth-induced dislocations.

2) Dislocations having irregular line directions due to post-growth motion but which still exhibit some characteristics of growth-induced dislocations.

3) Dislocations bearing little resemblance to growth dislocations and which have highly irregular line directions.

Categories 1) and 2) will be discussed first since any mechanism which explains the motion of the second category must also account for the lack of movement of the first.

5.2 Post-Growth Motion

The observed post-growth motion of the growth dislocations may be due to either climb or glide or to a combination of the two. Valuable indications of the nature of this motion are revealed by examining the dislocation configurations observed in the topographs and considering the probable line directions before motion took place.

5.2.1 Growth Dislocations with Irregular Line Directions

The dislocations labelled C in Figure 1 have Burger's vector [100] and lie in the {210} sectors Segments of these dislocations have undergone considerable motion to produce loops which lie in or very close to the plane of the slice, (010). Since the Burger's vector is [100], these observations are consistent with slip on the active slip plane, (010). However, for this dislocation, $\underline{b}$ and $\underline{n}$ are neither parallel nor orthogonal. It will be recalled that in such cases a dislocation is generally mixed and its line direction lies

between, and usually coplanar with, $\underline{b}$ and $\underline{n}$. Thus before motion took place, the entire dislocation line lay at an angle to the (010) slip plane (as shown in Figure 5a). Some initial motion was, therefore, required to bring segments of the line into this plane where they could subsequently expand by slip. There are two possible mechanisms for this initial motion, namely slip on an alternative slip plane, or climb. It will be noted from Figure 5a that although the dislocation originally lay at an angle to the (010) plane, it lies within the (001) plane. If slip were to occur on (001), segments of the dislocation line could be brought into the (010) plane as shown in Figure 5b. They would then be able to expand by slip on the (010) slip plane (Figure 5c). Because of the near equality of the interplanar spacings of (001) and (010), it is not unreasonable to propose that existing dislocations may slip on the former when they are unable to do so on the latter. Given such a situation one would not expect to observe (001) traces upon indentation. Additional evidence of the occurrence of (001) slip is provided by dislocation configurations to be discussed in 5.2.3.

The second possible mechanism for the initial motion is dislocation climb. Climb of these dislocations would result in motion normal to the (001) plane, i.e. normal to the plane containing $\underline{b}$ and $\underline{l}$. The resulting jogs would therefore contain line segments lying in the (010) slip plane as shown in Figure 6a. However, subsequent expansion of these segments by glide on (010) (Figure 6b) could not produce the observed dislocation configurations. We therefore suggest that the configurations of the dislocations C in Figure 1 are due to initial slip on (001) followed by cross-slip into, and expansion on (010).

The dislocations labelled B in Figure 1 have Burger's vector [001] and lie in the [111] growth sector. The observed configurations of these dislocations are characteristic of the transformation of dislocations with a screw component into helices. This is particularly noticeable at point B'. This is a process which is accepted to occur through a dislocation climb mechanism. In view of the low growth temperatures involved, one might intuitively expect relatively low point defect supersaturations and dislocation climb would therefore seem a remote possibility. However, as Hooper and Sherwood (1982) have shown in studies of α-sulphur, relatively small fluctuations in temperature ($\pm$0.3K) and hence growth rate can produce and trap the necessary supersaturation of point defects for dislocation climb to occur. This, together with enhanced diffusion of point defects along dislocation cores, characteristic of molecular solids (Chadwick and Sherwood 1975) can yield significant degrees of climb.

Unfortunately, no data are available for the rate of diffusion of point defects in the bulk or along dislocations in RDX, with which to test this proposal. We would not anticipate that self-diffusion in this solid would be greatly dissimilar to other molecular solids (Chadwick and Sherwood 1975). On this basis, at the growth temperature, T_g = 300K (T_g/T_m = 0.63 where T_m is the melting point), the rate of self-diffusion in the dislocations in RDX will be 10^2 lower than in α-sulphur (T_g/T_m = 0.78). As a result, smaller helices will develop in RDX. Further supporting evidence comes from the observation that the

helices narrow as growth proceeds. For a constant imposed precipitation rate, the linear growth rate in a given growth sector decreases as the crystal grows larger. Thus one might expect a decrease in the degree of trapping of point defects with time and hence climb to become less extensive.

5.2.2 Straight Growth Dislocations

The dislocations labelled A in Figure 1 are pure edge in character, lie in the (210) growth sector and like those labelled B have Burger's vector [001]. However, unlike the latter dislocations, those labelled A have remained essentially straight throughout their length. The lack of motion by glide is a direct result of the character of these dislocations. Since they lie at an angle to the (010) slip plane, these dislocations must undergo some form of initial motion before they could glide on this plane. However, it is impossible for these dislocations to undergo glide on any alternative slip plane since the Burger's vector, [001], does not lie in any of the possible alternatives; (001), (021) or (011) (Halfpenny, Roberts and Sherwood (1984b)). Furthermore, if the dislocations climb, the resulting jogs have no line segments lying in the (010) slip plane, as shown in Figure 7. Thus, in either case, the dislocations cannot move into the (010) slip plane and therefore cannot expand by glide on that plane. The absence of pure climb in this case to form helices is attributed to the slower growth rate of the {210} growth sectors which results in less extensive trapping of point defects during growth.

Similar arguments apply to the dislocation labelled E in Figure 1 which also shows no evidence of post-growth motion. The Burger's vector is <011> and the dislocation is inclined to the (010) slip plane both before and after crossing the growth sector boundary. Again the Burger's vector does not lie in any of the alternative slip planes and dislocation climb does not produce any line segments lying in (010). It will be recalled that the helices discussed above narrowed or became linear in the latter stages of crystal growth. The location of dislocation E leads us to believe that the absence of observable pure climb in this case is due to a similar cause.

5.2.3 Dislocations having Highly Irregular Line Directions

The dislocations labelled F in Figure 3 have very irregular line directions and show none of the features usually associated with growth induced dislocations. One might therefore assume that these dislocations were introduced mechanically. However, the Burger's vector is [010] and since this does not lie on the (010) slip plane, it is impossible for the dislocations to have been introduced by plastic deformation on this plane. While it is highly probable that existing dislocations may be able to glide on alternative planes, as discussed above, it seems unlikely that dislocations could be introduced by deformation on slip planes other than those revealed by microhardness indentation. We therefore believe these dislocations to be growth induced. Again, by virtue of the Burger's vector the observed configurations cannot be due to glide on (010). This leaves two possibilities, namely glide on the alternative (001) slip plane or pure climb. It is not clear which of these two mechanisms is responsible. The extent of the post-growth motion, however, tends to favour a glide mechanism.

A similar situation is encountered with the dislocations labelled D in Figure 1. The Burger's vector is <110> and they are therefore considered to be growth induced for the reasons described above. The irregular line directions may again be due to either glide on (001) or pure climb.

6. CONCLUSION

In conclusion, the major points of this study may be summarized thus:-

a) The theoretically possible growth dislocation types have been deduced for the dominant {210} and {111} growth sectors of RDX crystals.

b) Solution grown crystals of RDX have been examined by X-ray topography. The predominant dislocation types have been characterized and have been found to comprise the following Burger's vectors:

[001], [100], [010], <011> and <110>

c) Many of the observed dislocations exhibit extensive post-growth motion. A few remain straight.

d) Dislocation helices have been observed, thus indicating the occurrence of dislocation climb.

e) The existence of an additional slip plane, (001), is proposed. The motion of existing dislocations on such a plane is considered highly probable in view of the near-equality of the relevant inter-planar spacings.

f) Other instances of post-growth motion are interpreted in terms of a combination of glide on the primary (010) slip plane preceded either by glide on (001) or by climb.

Mechanical deformation studies are in course to assess the reliability of these conclusions.

ACKNOWLEDGEMENTS

We express our grateful thanks to the European Office of the US Army (USARDSG-UK) for their financial support of this work.

REFERENCES

Afanasev, G.T. and Bobolev, V.K. (1971) Initiation of Solid Explosives by Impact, Jerusalem, Israel Program for Scientific Translations.

Bhat, H.L., Roberts, K.J. and Sherwood, J.N. (1983), J. Appl. Cryst., 16, 390.

Bowden, F.P. (1958) Proc. Roy. Soc., A246, 146.

Chadwick, A.V. and Sherwood, J.N. (1975) in: Point Defects in Solids, Vol. 2, Eds. Crawford, J.H. and Slifkin, L. (Plenum, New York) Ch. 6.

Choi, C.S. and Prince, E. 1972, Acta Cryst., A28, 2857.

Coffey, C.S. (1981), Phys. Rev., B24.

Coffey, C.S. and Armstrong, R.W. (1981) in: Shock Waves and High Strain Rate Phenomena in Metals: Concepts and Applications, Eds. Meyers, M.A. and Muir, L.E.(Plenum, New York).

Connick, W. and May, F.G.J. (1969) J. Crystal Growth, 5, 165.

Elban, W.L. and Armstrong, R.W. (1981) 7th International Symposium on Detonation, Annapolis, Maryland (US ONR).

Field, J.E., Swallow, J.M. and Heavens, S.N. (1982) Proc. Roy. Soc., A382, 231.

Gross, K. (1970), J. Crystal Growth, 6, 210.

Halfpenny, P.J. (1982), PhD Thesis, University of Strathclyde.

Halfpenny, P.J., Roberts, K.J. and Sherwood, J.N. (1984a), J. Crystal Growth, submitted.

Halfpenny, P.J., Roberts, K.J. and Sherwood, J.N. (1984b), J. Materials Sci., in press.

Halfpenny, P.J., Roberts, K.J. and Sherwood, J.N. (1984c), J. Appl. Cryst., in press.

Herley, P.J. and Levy, P.W. (1972) in: Reactivity of Solids, Proc. 7th Intern. Symp., Eds. Anderson, J.S., Roberts, M.W. and Stone, F.S. (Chapman and Hall, London) p. 387.

Hooper, R.M. and Sherwood, J.N. (1982), Phil. Mag. A46, 559.

Jach, J. (1962) Nature, 196, 827.

Klapper, H. (1972), Phys. Stat. Sol. (a), 14, 443.

Klapper, H. (1973), Z. Naturforschung, 28a, 614.

Klapper, H., Fishman, Y.M. and Lutsau, V.G. (1974) Phys. Stat. Sol. (a) 21, 115.

Klapper, H. (1980) in: Characterization of Crystal Growth Defects by X-ray Methods, Eds. Tanner, B.K. and Bowen, D.K. (Plenum, New York) p. 133.

Lang, A.R. (1962), unpublished work referred to in Lang (1978).

Lang, A.R. (1978) in Diffraction and Imaging Techniques in Material Science (Eds. Amelinckx, Gevers, Remaut and Van Landuyt), North Holland, Amsterdam, p.623.

McDermott, I.T. and Phakey, P.P. (1971a) Phys. Stat. Sol. (a) 8, 505.

McDermott, I.T. and Phakey, P.P. (1971b) J. Appl. Cryst., 4, 479.

Meyer, W., Lieser, G. and Wegner, G. (1978), J. Polymer Sci. Polymer Phys. Ed.,16, 1365.

Singh, K. (1956) Trans. Faraday Soc., 52, 1623.

Thomas, J.M. (1969), Advances in Catalysis, 19, 293.

Winter, R.E. and Field, J.E. (1975), Proc. Roy. Soc., A343, 399.

FIGURE CAPTIONS

Figure 1 Schematic diagram of the (010) RDX crystal slice shown in the topographs in Figure 2, scale mark 1mm.

Figure 2 X-ray topographs of an (010) RDX crystal slice. (a) 200, (b) 102, (c) 002, (d) $4\bar{2}0$, (e) $0\bar{2}3$, and (f) $2\bar{2}0$ reflections.

Figure 3 Schematic diagram of the (001) RDX crystal slice shown in the topographs in Figure 4. Scale mark 1mm.

Figure 4 X-ray topographs of an (001) crystal slice. (a) 200 and (b) 040 reflections.

Figure 5 Cross slip mechanism involving the additional glide plane (001),for dislocations labelled C, $\underline{b}$ [100].

Figure 6 Combined climb and slip mechanism for dislocations labelled C, $\underline{b}$ [100].

Figure 7 Climb produced jogs on the pure edge dislocations labelled A with $\underline{b}$ [001].

$\underline{b}$	$\lvert\underline{b}\rvert$ (nm)
[001]	1.0709
[010]	1.1574
[100]	1.3182
⟨011⟩	1.5768
⟨101⟩	1.6984
⟨110⟩	1.7542
⟨111⟩	2.0553

Table 1

RDX Burgers Vectors

$\underline{b}$	Growth Sector	Character	Comments
[001]	(210)	Edge	parallel to $\underline{n}$
	(111)	Mixed	lies in 110
[010]	(210)	Mixed	lies in (001)
	(111)	Mixed	
[100]	(210)	Mixed	lies in (001)
	(111)	Mixed	
⟨011⟩	(210)	Mixed	
	(111)	Mixed	
	(11$\bar{1}$)	Edge	
⟨101⟩	(210)	Mixed	
	(111)	Mixed	
	(11$\bar{1}$)	Edge	
⟨110⟩	(210)	Mixed	
	(111)	Mixed	
	($\bar{1}$11)	Edge	

Table 2

Theoretically possible growth dislocation types in the {210} and {111} growth sectors of RDX crystals.

$\underline{b}$	Growth Sector	Configuration	Likely Character
[001]	{210}	Straight	Edge
[001]	{111}	Helices	Mixed
[010]	{111}	Irregular	Mixed
[100]	{210}	Irregular	Mixed
⟨011⟩	{111}	Straight	Mixed
⟨110⟩	{210}	Irregular	Mixed

Table 3

Observed dislocation types in RDX.

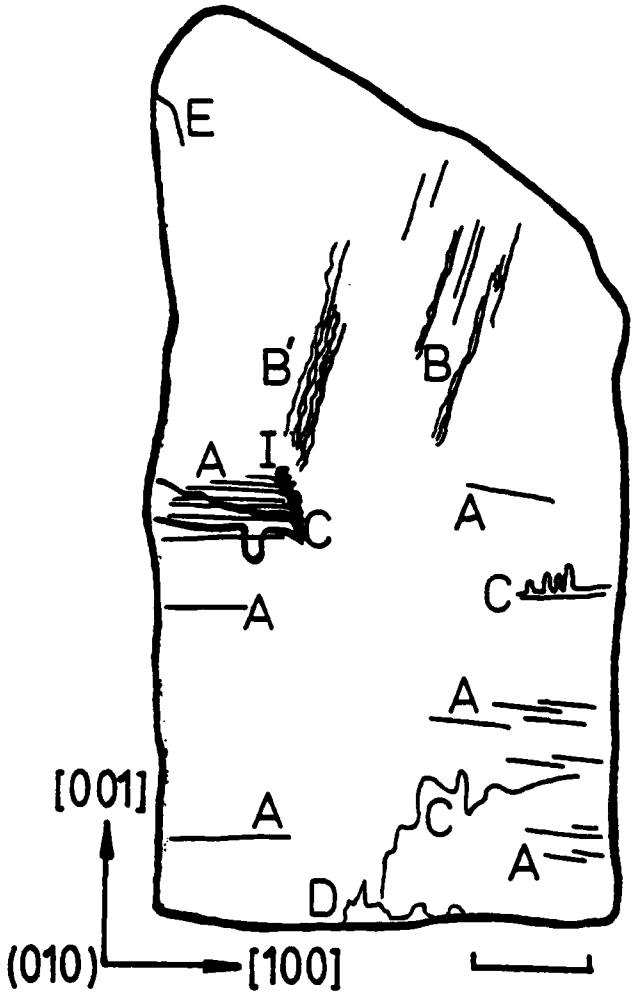

FIGURE 1

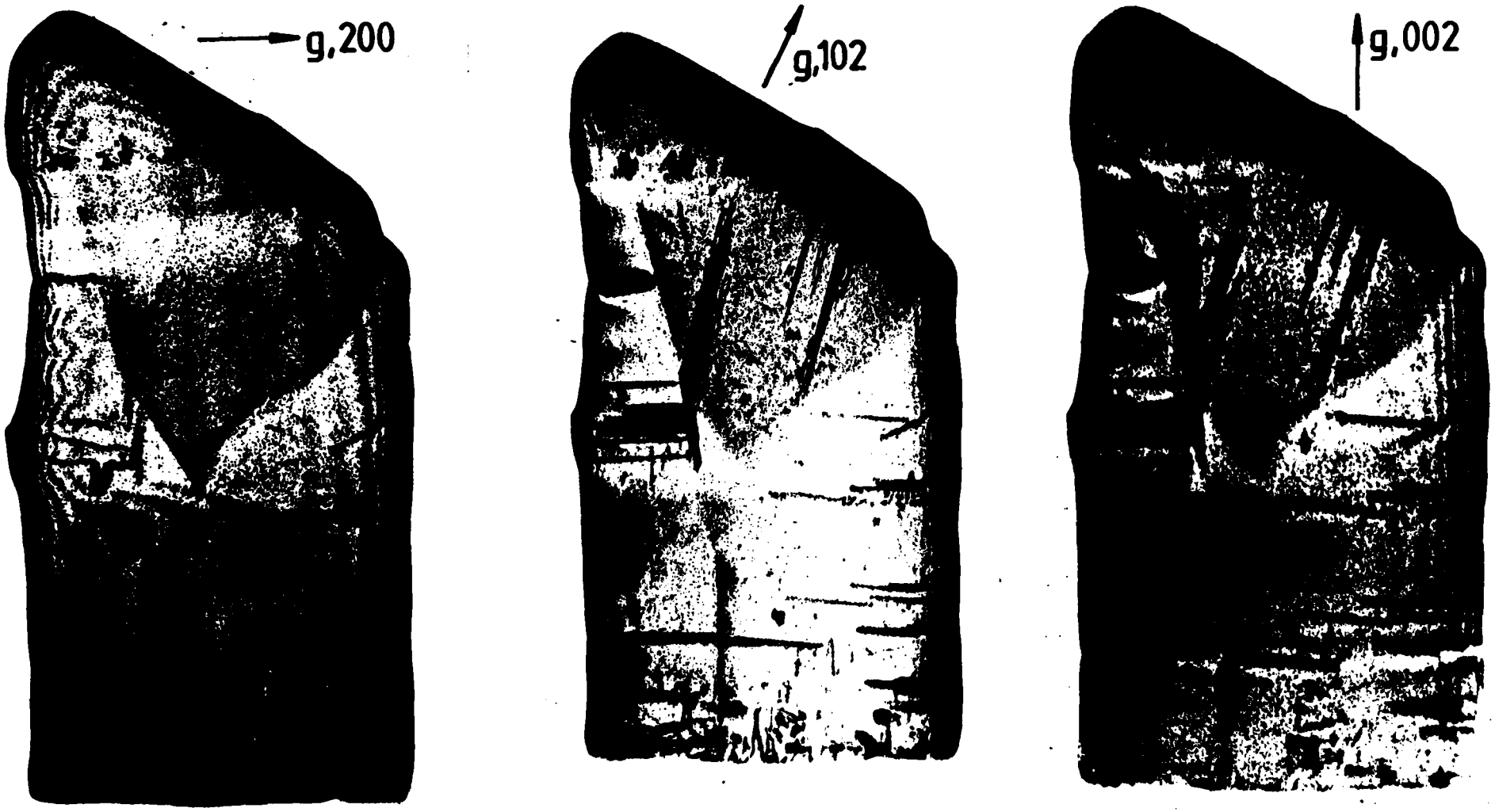

a b c

FIGURE 2

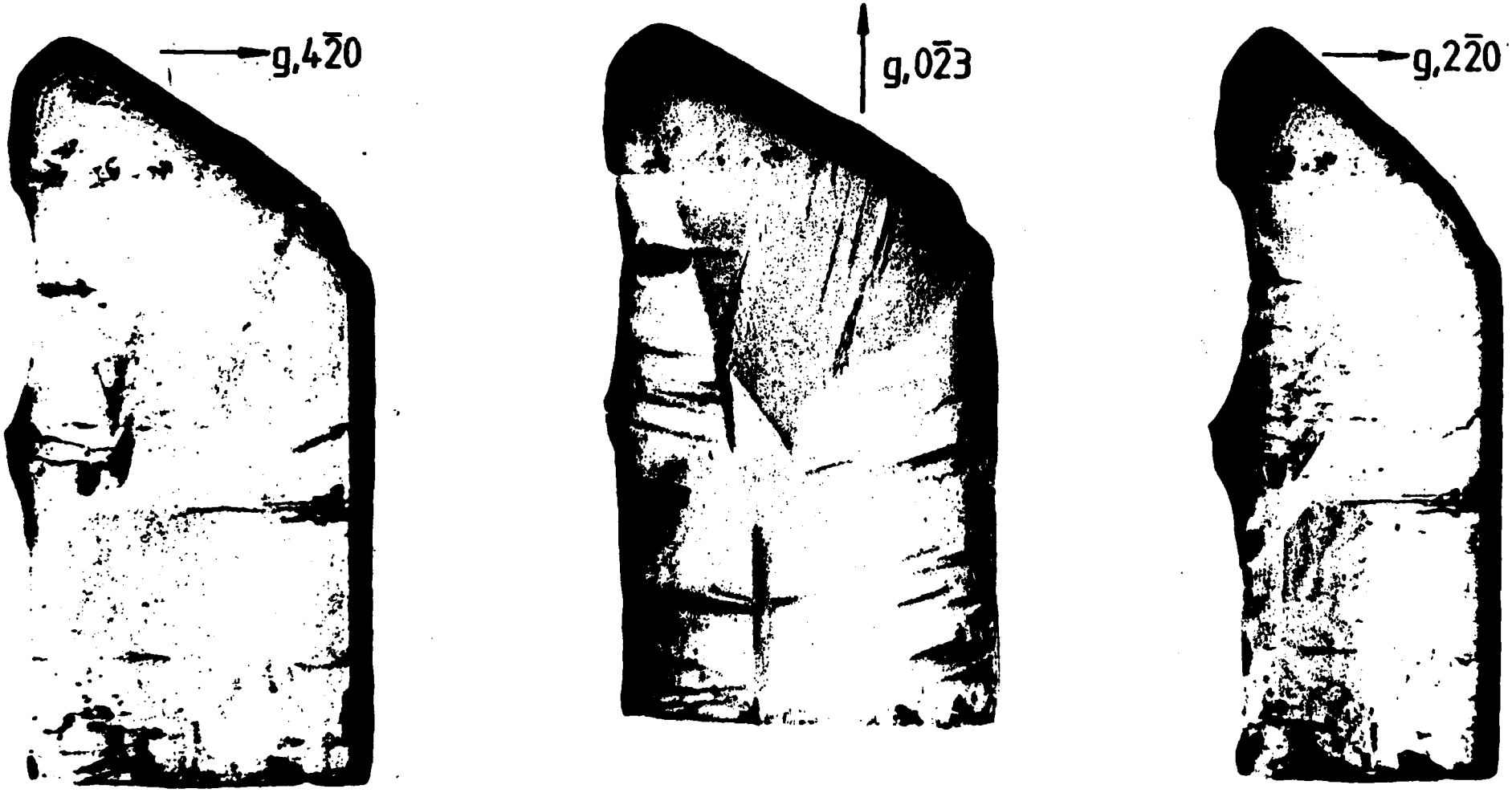

d e f

FIGURE 2

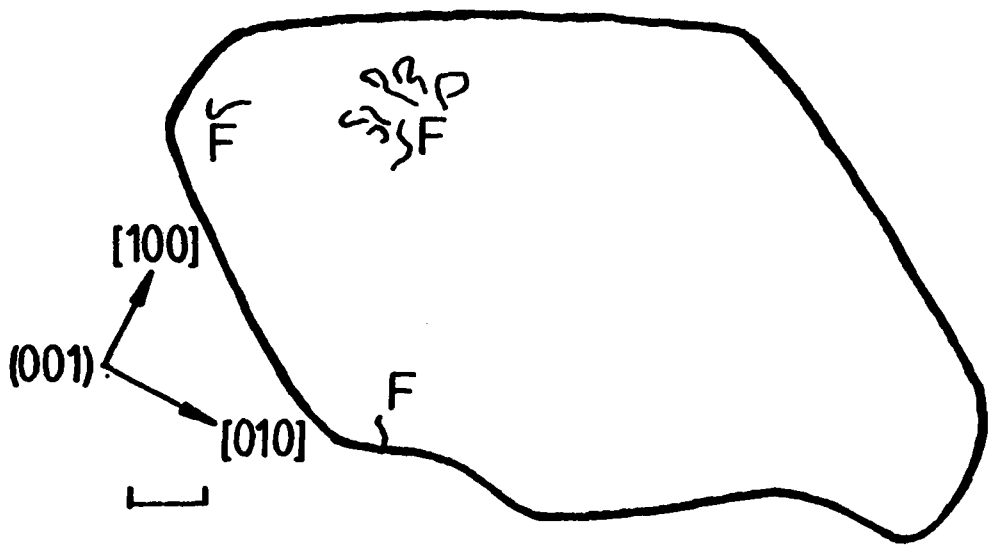

FIGURE 3

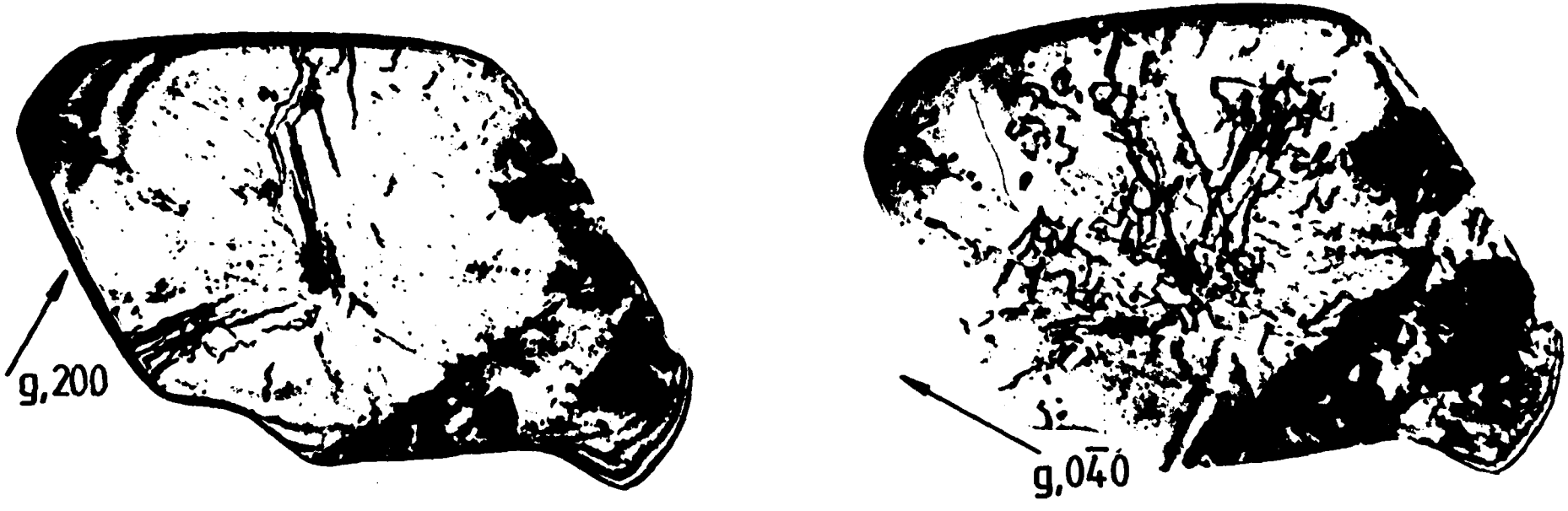

FIGURE 4

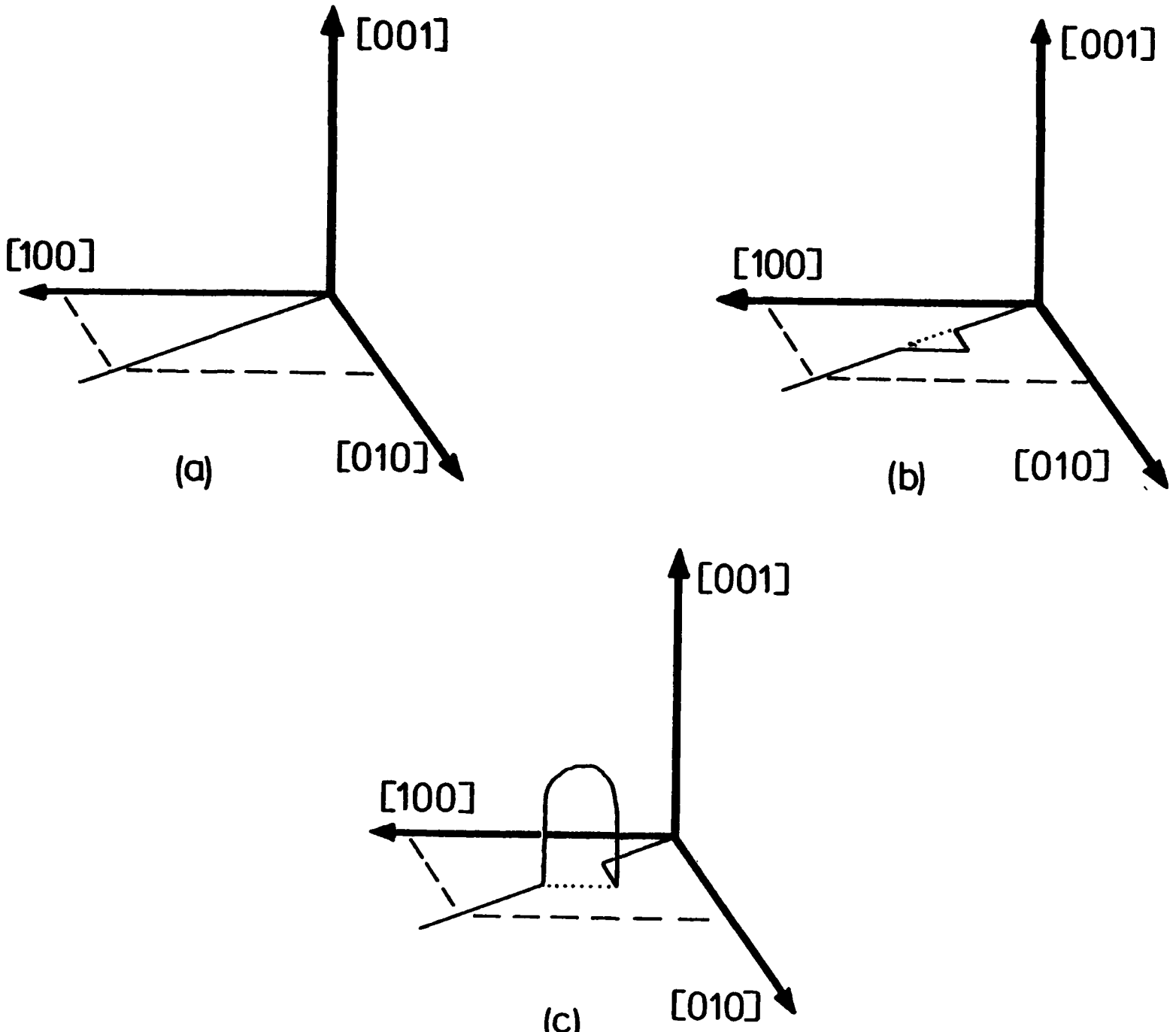

FIGURE 5

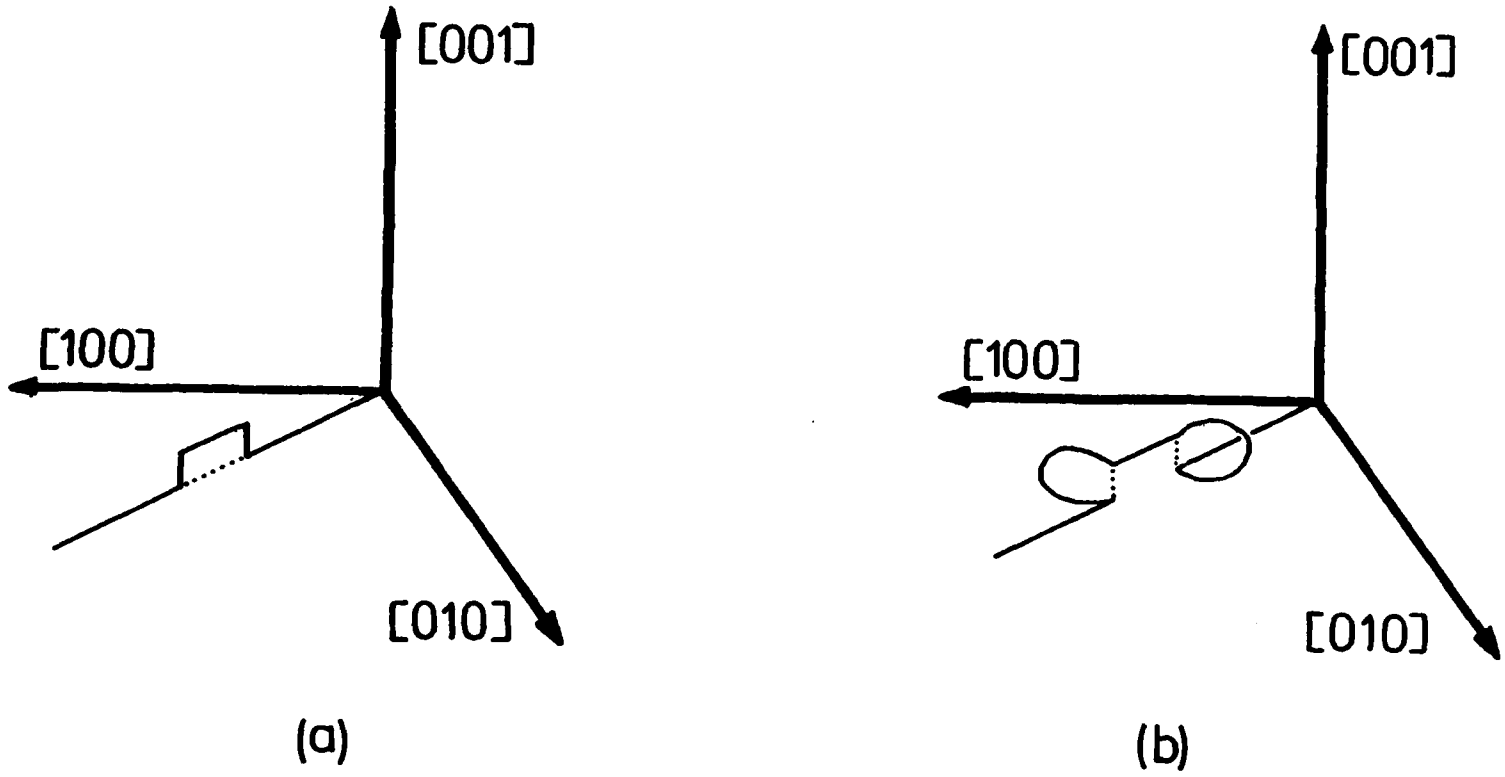

FIGURE 6

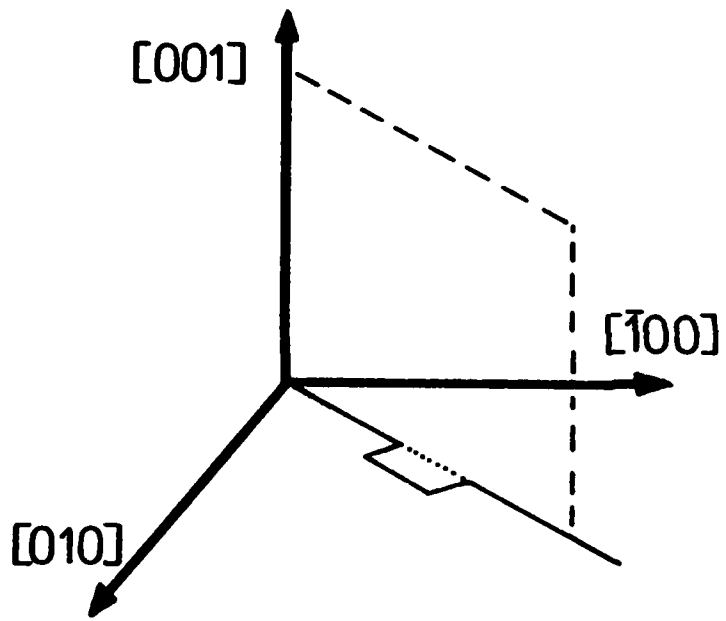

FIGURE 7

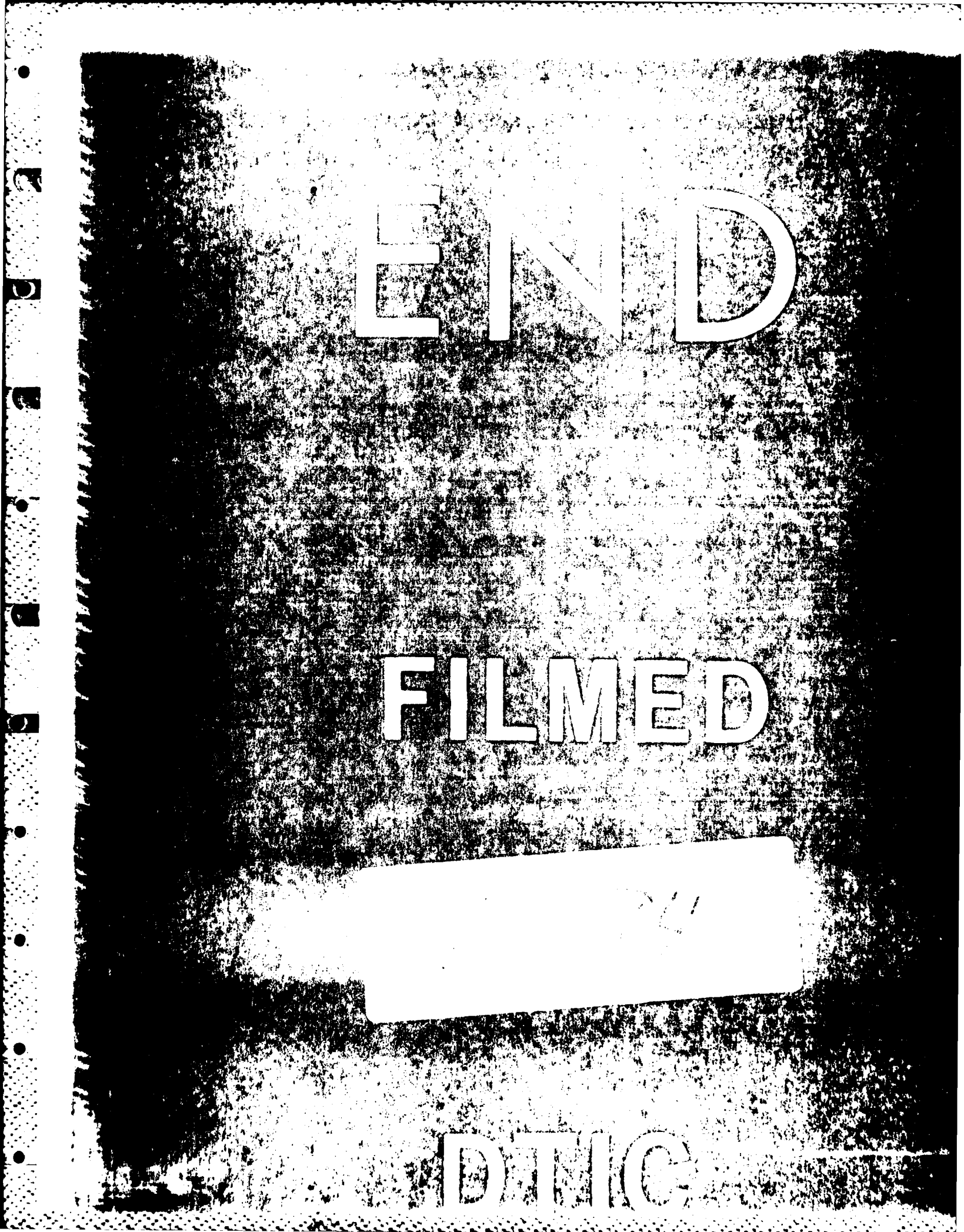
END
FILMED
DTIC